Czech Technical University in Prague
Faculty of Civil Engineering
Department of Concrete and Masonry Structures

NUMERICAL ANALYSIS

OF CONCRETE BIOLOGICAL SHIELD

by

Bc. Jiří Kovář

A master's thesis submitted to
the Faculty of Civil Engineering, Czech Technical University in Prague,
in partial fulfilment of the requirements for the degree of Master of Science.

Master degree study programme: Civil Engineering
Specialization: Building Structures

Prague, January 2023

Title of the thesis:
Numerical Analysis of Concrete Biological Shield

Student:
Bc. Jiří Kovář
E-mail: jiri.kovar@fsv.cvut.cz

Supervisor:
Mgr. Yuliia Khmurovska, Ph.D.
E-mail: yuliia.khmurovska@fsv.cvut.cz
Department of Concrete and Masonry Structures
Faculty of Civil Engineering
Czech Technical University in Prague
Thákurova 2077/7
166 29 Praha 6
Czech Republic

ČESKÉ VYSOKÉ UČENÍ TECHNICKÉ V PRAZE
Fakulta stavební
Thákurova 7, 166 29 Praha 6

ZADÁNÍ DIPLOMOVÉ PRÁCE

I. OSOBNÍ A STUDIJNÍ ÚDAJE

Příjmení: Kovář Jméno: Jiří Osobní číslo: 477148

Zadávající katedra: K133

Studijní program: Stavební inženýrství

Studijní obor/specializace: Konstrukce pozemních staveb

II. ÚDAJE K DIPLOMOVÉ PRÁCI

Název diplomové práce: Numerická analýza betonového prstence biologického stínění

Název diplomové práce anglicky: Numerical Analysis of Concrete Biological Shield

Pokyny pro vypracování:
Axisymetrická nelineární formulace MKP modelu

Validace parametrů modelu poškození

Vytvoření numerického kódu

Příklad aplikace

Seznam doporučené literatury:
Internetové zdroje

Jméno vedoucího diplomové práce: Mgr. Yuliia Khmurovska, Ph.D

Datum zadání diplomové práce: 27.9.2022 Termín odevzdání DP v IS KOS: 9.1.2023
Údaj uveďte v souladu s datem v časovém plánu příslušného ak. roku

Podpis vedoucího práce Podpis vedoucího katedry

III. PŘEVZETÍ ZADÁNÍ

Beru na vědomí, že jsem povinen vypracovat diplomovou práci samostatně, bez cizí pomoci, s výjimkou poskytnutých konzultací. Seznam použité literatury, jiných pramenů a jmen konzultantů je nutné uvést v diplomové práci a při citování postupovat v souladu s metodickou příručkou ČVUT „Jak psát vysokoškolské závěrečné práce" a metodickým pokynem ČVUT „O dodržování etických principů při přípravě vysokoškolských závěrečných prací".

27.09.2022
Datum převzetí zadání Podpis studenta(ky)

Declaration

Author:

Jiří Kovář

Title of the thesis:

Numerical Analysis of Concrete Biological Shield

I declare that this thesis was composed by myself, that the work contained herein is my own except where explicitly stated otherwise in the text, and that this work has not been submitted for any other degree or processional qualification except as specified.

. . . . . .

Jiří Kovář

In Prague, January 2023

Abstract

The goal of this Master's thesis is to conduct an analysis of a concrete biological shield exposed to the effect of radiation using an axisymmetric numerical model analysed by finite element method.

The first part of the work briefly summarizes theory of the radiation originating from nuclear fission in a nuclear reactor and types of this radiation are described. The importance of gamma and neutron radiation in the context of concrete is presented. Heavy concretes used for shielding and the radiation's effect on them are introduced.

The main part of the thesis describes a numerical model of a concrete biological shield of reactor VVER 440/213 using MATLAB software. Axisymmetric model of CBS is assumed and analysed using Mazars' μ damage model to determine formation and development of damage of the structure.

Keywords: concrete exposed to radiation, concrete biological shield, finite element method, axisymmetric numerical model

Abstrakt

Cílem této práce bylo provést analýzu betonového prstence biologického stínění vystaveného vlivu radioaktivního záření. Analýza byla provedena použitím metody konečných prvků na uvažovaný axisymetrický numerický model prstence.

První část práce stručně shrnuje teorii vzniku záření při jaderném štěpení v jaderných elektrárnách a popisuje typy těchto záření. Je uvedena důležitost uvážení gama a neutronového záření ve spojení s betonem. Dále jsou popsány těžké betony používané pro stínění záření a vliv tohoto záření na jejich vlastnosti.

Hlavní část práce popisuje vytvořený numerický model betonového prstence biologického stínění reaktoru VVER 440/213 s použitím výpočetního programu MATLAB. Je předpokládán axisymetrický model prstence, jenž je následně analyzován s použitím Mazarsova μ modelu poškození ke zjištění vzniku a následného rozvoje poškození konstrukce vystavené vlivu záření.

Klíčová slova: beton vystavený radioaktivnímu záření, betonový prstenec biologického stínění, metoda konečných prvků, axisymetrický numerický model

Acknowledgement

My deepest gratitude belongs to my academic supervisor Mgr. Yuliia Khmurovska, Ph.D. for her endless patience and goodwill to help me understand all kinds of problems during studying a new topic, which always allowed me to progress in learning new things that I enjoy. I appreciate all the time she devoted to providing consultation and giving me countless pieces of advice.

Last but not least, I would like to express my gratitude to prof. Ing. Petr Štemberk, Ph.D., D.Eng. for not turning his back on me when I addressed him. Instead, helped me find the right path, sort of speak, of what I want to do in the future work even when I myself did not know what it exactly was at the time.

Lastly, I cannot leave out thanking to my beloving mother, who stood behind me all those years during study, providing support in all the ways necessary. Without her, I would have hardly get through everything during the years of my study.

Contents

List of Figures

Symbols

$\mathbf{A}$	"Border" of the global stiffness matrix
A	Variable including the quasi-fragile behavior of the concrete
A_c	Parameter shaping the Mazars' damage model
A_t	Parameter shaping the Mazars' damage model
B	Variable including the quasi-fragile behavior of the concrete
B_c	Parameter shaping the Mazars' damage model
B_t	Parameter shaping the Mazars' damage model
$\mathbf{B}$	Matrix of derivatives of the shape functions
$\mathbf{D}$	Material matrix
d	Isotropic damage
$\mathbf{df}$	Residuum/Difference between internal and external forces
E	Young's modulus of elasticity
$\mathbf{f}$	Global vector of external forces
$f_{CG}^{(e)}$	Body force of an element
f_{att}	Neutron flux inside the CBS including attenuation
f_{surf}	Neutron flux on the inner surface of the CBS

$\mathbf{f^{(e)}}$	Local vector of forces
f_c	Ultimate compression strength
f_t	Tension strength
I_ε	First invariant of the strain tensor
J_ε	Deviatoric part of the strain tensor
$\mathbf{K}$	Global stiffness matrix
$\mathbf{k}^{(e)}$	Local stiffness matrix of an eth element
k	Parameter shaping the Mazars' damage model
$\mathbf{p}$	Vector of prescribed displacements
$P(u)$	Internal force as a function of displacement
$\mathbf{P}$	Vector of internal forces
r	Triaxial factor
$\bar{r}$	Radial coordinate of the center of mass of an element
$\sum_R$	Effective removal cross-section
$\mathbf{u}$	Global vector of displacements
u_0	Initial displacement
u_{lin}	Linear displacement
u^i	Displacement at the ith iteration
u^{i+1}	Displacement in the next iteration
x	Depth into the CBS
Y	Driving damage variable depending on the equivalent strains
Y_0	Initial threshold for Y
Y_c	Maximum compressive strain reached during loading
Y_t	Maximum tensile strain reached during loading
$\bar{z}$	Vertical coordinate of the center of mass of an element
$\alpha, \beta, \gamma_{i,j,m}$	Values of derivarives of shape functions in an element's vertices
γ_{rz}	Shear strain
Δu	Displacement increment

δ	Inverse of a fluence governing the shape of the RIVE function
$\{\boldsymbol{\varepsilon}\}$	Strain tensor
$\boldsymbol{\varepsilon}$	Strain vector
ε_r	Strain in radial direction
ε_z	Strain in the vertical direction
ε_{cir}	Strain in the circumferential direction
ε_{RIVE}	Strain caused by RIVE
ε_{max}	Maximum expansion caused by RIVE
ε_c	Equivalent compression strain
ε_t	Equivalent tension strain
ε_{c0}	Initial compression strain threshold
ε_{t0}	Initial tension strain threshold
κ	A dimensionless parameter homogeneous to a strain
$\boldsymbol{\lambda}$	Vector of Lagrange multipliers
λ	Lagrange multiplier
ν	Poisson's ratio
Φ	Neutron fluence
ρ	volumetric mass
$\boldsymbol{\sigma}$	Stress vector
σ_r	Stress in radial direction
σ_z	Stress in vertical direction
σ_{cir}	Stress in circumferential direction
$\sigma_{1,2}$	Principal stresses
$\sigma_{damaged}$	Stress after damage correlation
τ_{rz}	Shear stress
Ω	Whole area of interest (volume of the structure)
$\langle\cdot\rangle^+$	Positive components
$\lvert\cdot\rvert$	Absolute value
M^T	Transpose of a matrix

CHAPTER 1

Introduction

History of nuclear energy goes all the way back to the first half of the 20th century, when, mostly thanks to Enrico Fermi and later a team of German scientists, the heavy nuclei fission was clarified. Thanks to this discovery, an era of nuclear power has begun, not only for weapons, but for energy too. By the year 1942, the first nuclear reactor was build in Chicago by a team led by Enrico Fermi.

By the second half of 20th century, a Golden Age of energy started big growth of nuclear power plants (NPPs) for commercial manufacture of electricity. In Europe, most of the nuclear NPPs were build in the 70s and 80s. Nowadays, nuclear power still represents a large topic worldwide and it is one of the most productive sources of electricity manufactures (e.g. in Czech Republic, nearly 40 % of electricity is manufactured in nuclear power plants).

After the Chernobyl incident and maybe even more after the earthquake in Tohoku in Japan, safety of NPPs became a very discussed topic of modern society. As of 2022, the world's nuclear fleet consists of a total of 411 reactors worldwide with an average age of 31 years (see Fig. 1.1) [1]). Originally designed operating life-time of a reactor is $\approx$ 30 years (20 to 40 years varying in different countries),

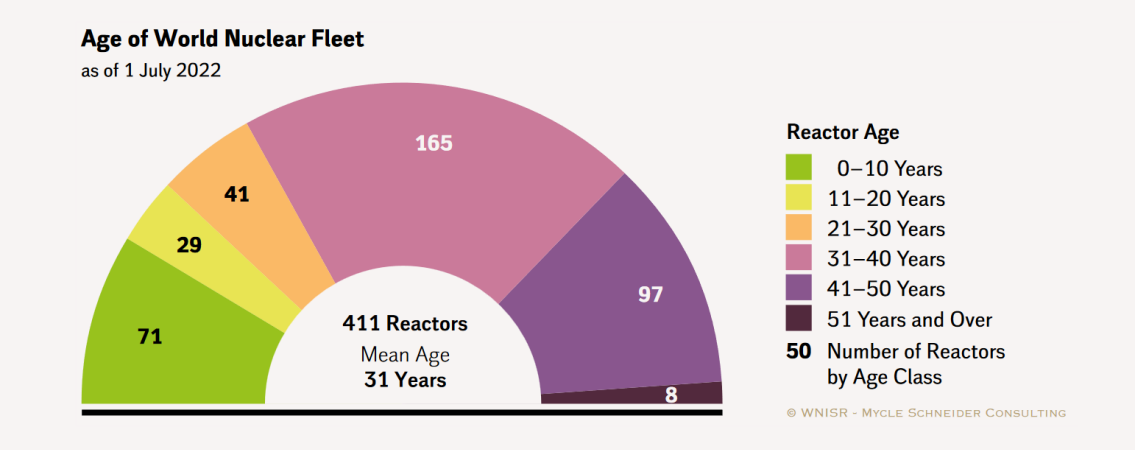

Figure 1.1: Age of World Nuclear Fleet

after which the reactor is condemned for decommission or a renewal of the operating license must be evaluated. This process includes mostly the safety evaluation of the reactor, in order to assess if the radiation does not lead to life-threatening risks.

Mentioning concrete in the context of nuclear power plants, probably the most common idea that comes to mind is the cooling towers. However, in the complex of NPP, there are more concrete structures with no less importance; load-bearing structures supporting the reactor pressure vessels, whole containment building mostly made of prestressed concrete or the concrete biological shields (which is the main topic of this thesis). Concrete biological shield represents the primary barrier separating reactor's active zone from its surroundings, capturing the gamma and neutron radiation.

The most important requirement when it comes to concrete shielding structures is their soundness. The risk of tightness breach is represented by formation and following development of cracks during the lifetime of the structure. After a crack exceeds a limit value of width or depth, it starts to compromise the concrete's shielding properties; consequently, loses its purpose which brings the structure to the end of its lifespan. Therefore, cracks represent the major role when stating the lifetime of shielding structure (or assessing extending the originally designed lifetime and providing the operating license renewal). The prospect of extending operation of nuclear power plants beyond 60 years raises critical questions

about the structural integrity of the concrete biological shield against prolonged neutron and gamma irradiation [2].

The main part of this Master's thesis is an analysis of a concrete biological shield of a VVER 440/213 reactor, focused on the damage development through years of operation. These structures are non-load-bearing (except for self-weight), and thus the primary load is the aggressive environment - radiation, high temperature and moisture. In this work, only the effects of **RIVE** (**R**adiation-**I**nduced **V**olumetric **E**xpansion of the aggregate - described in Chapter 2.2.1) and self-weight are taken into consideration. For this purpose, a numerical model was created using finite element method. Non-linear behavior of concrete was described using Mazars' μ damage model and the modified Newton-Raphson iteration method was used for the non-linear analysis. More detailed description of the whole procedure is in Chapter 3.

In the last chapter (Chapter 4), the results are presented. Four analyses on the similar topic conducted in recent years are introduced and compared to the created model.

CHAPTER 2

Radiation and its Effect on Concrete

2.1 Radiation in nuclear reactors

In a nuclear power plant, the nuclear fission takes place. As a nuclear fuel, the enriched uranium (in Czech Republic, only the uranium ^{235}U is used) is placed in a zirconium-alloy-bar. The uranium nucleus is a target for a projectile in a form of neutrons. These neutrons need to be moderated in order to successfully hit the uranium nucleus. After the neutron-nucleus collision, an excited and very unstable compound nucleus of ^{236}U is formed. The compound then fissions into two nuclear products and two or three fast immediate neutrons, these neutrons are again moderated, continuing in the process, inducing the chain mechanism and undergo another nuclear fission (see Fig. 2.1). The fission products, on the other hand, are fragments nuclei left of the large uranium nucleus after the collision. It is never known with certainty what elements are these items going to be representing, they are determined according to the fuel-element's decay chain and their decay is eventually the primary source of all types of radiation.

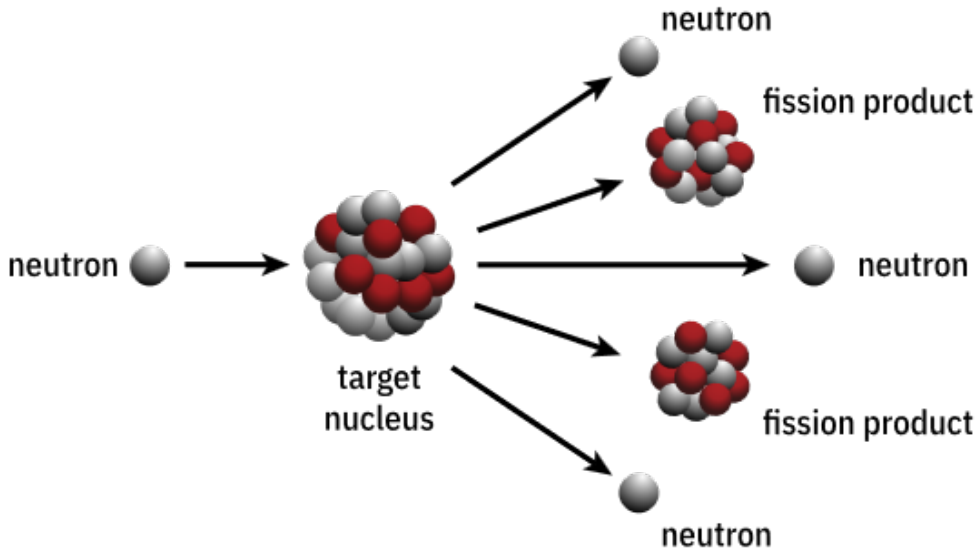

Figure 2.1: Nuclear fission schema

Basically, there are four essential types of radiation: alpha, beta, gamma and neutron (see Fig. 2.2). On topic of concrete biological shield (or the whole complexity of the problem of irradiated concrete), only the gamma and neutron radiation are relevant to take into account for the reasons explained below.

Alpha decay represents relatively small danger because the effect of alpha radiation can be neglected by its characteristically high linear energy transfer. An α particle is a helium nucleus. The nucleus is carrying four times the mass of a neutron and double the electric charge of a β particle. Consequently, it is affected by electromagnetic and strong nuclear forces more than the other types of nuclear radiation, which allows countless materials to capture it almost immediately. This is often illustrated by a paper sheet being able to eliminate α radiation. Therefore, the α radiation is irrelevant in relation to concrete shielding.

Two types of β decay can be distinguished, β^- and β^+. In the case of β^- decay, the β particle is a proton emitted together with an antineutron in the process of neutron transforming into a proton. Conversely, less common decay in nuclear fission, β^+ is a process of a proton becoming a neutron by emitting a positron and a neutrino. Neutrinos or antineutrinos have a very low to none potential

of interaction with any mass. However, the electrons are directly ionizing particles interacting with environment. β particles' mass is much smaller compared to the alpha ones and they move much faster as well, but their interaction with the environment caused by non-zero charge allows many materials to shield the radiation without a problem. That means the β radiation does not need to be considered during concrete shielding properties evaluation as well as α radiation.

Unlike the α and β, the γ decay produces an electromagnetic radiation. The fission product or another nucleus stays in a very excited state and its structure remains the same. This nucleus then tries to get into a state with less energy, so it emits a ray of photons, which is considered as γ radiation. The γ particles can be called a photon. Photon, by its definition, has no electric charge so it does not interact with matter, but the particles are moving very fast and thus have a significant kinetic energy. Therefore, a very heavy element (dense materials) is needed for "capturing" it. This role partly belongs to the reactor's steel pressure vessel. However, it cannot capture all of it, so some of the γ radiation penetrates the pressure vessel, affecting the CBS. To describe the intensity of γ radiation, two quantities are usually used: *energy dose*, which correspond to the total amount of energy absorbed by a unit mass and *dose rate* that indicates the amount of absorbed energy per a time unit (basically energy dose per time) [3].

Neutron radiation is fairly self-descriptive. It is a flow of free neutrons emitted from nuclei with surplus of neutrons in comparison with protons. Different kinds of neutron radiation can be distinguished based on energy of the neutron. In case of shielding neutron radiation with concrete, two main types are important to consider; fast neutron ($energy > 0.1\,MeV$) and slow or thermal neutrons ($energy < 0.1\,MeV$) [4] (the necessary approach for shielding the different types is described in more detail in the next section (Chapter 2.2).

Fast neutrons (high-energy) are relatively heavy particles (their mass is not far from the mass of α particles - exactly one fourth), but they have no electric charge, therefore they do not interact with matter and they are able to travel fairly long

distances. These neutrons need to be slowed down, which is carried out by using materials containing a lot of hydrogen atoms, called moderators (typical moderator is light or heavy water or solid graphite). During the process of slowing and absorbing neutrons, their kinetic energy is converted into heat and the secondary gamma rays are emitted.

Two quantities are commonly used to describing the intensity of neutron radiation. The *neutron flux* and *neutron fluence*. The neutron flux indicates the amount of neutrons that penetrate a cross-section of a sphere with area 1 cm^2 during 1 *second*. The neutron fluence is virtually time integral of flux, therefore it corresponds to the total number of neutrons penetrating the cross-section [3].

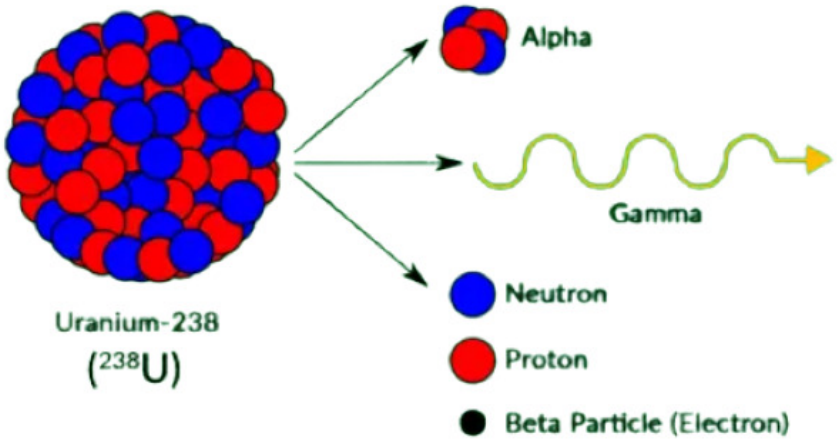

Figure 2.2: Types of radiation decay

2.2 Radiation-shielding concrete

For the reasons given in the previous section, two types of radiation need to be considered when designing or analysing the radiation-shielding concrete; gamma and neutron radiation (see Fig. 2.3). In this section, the reasons why concrete is a good shielding material are given as well as a brief explanation of how it is affected during years of exposure.

Concrete is a homogeneous mixture of compounds able to provide an effective

shielding properties for both radiations mentioned, γ and neutron. The heavy part of the material, represented usually by aggregates, can attenuate the γ rays and fast neutrons. On the other hand, chemically bound water in cement paste (or contained in the chosen aggregates) provides a sufficient quantity of hydrogen to slow down and absorb thermal neutrons. Therefore, in a shielding concrete composition, designed to provide the highest attenuation of gamma and neutron radiation, a delicate balance between the proportion of high density aggregate and the components, which contain hydrogen in a form of chemically bound or adsorbed water must be achieved [4].

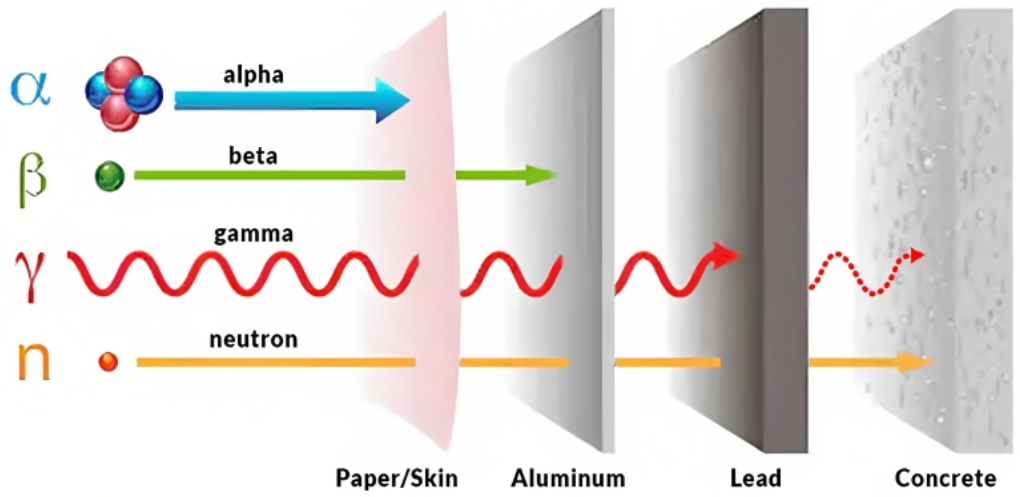

Figure 2.3: Schema of penetrating power of different radiation types

Heavy concrete used for shielding radiation finds use in more fields than just the nuclear power plants; it is often used in radiation workplaces of medical facilities, non-destructive testing facilities, etc. By mentioning a heavy concrete, a concrete with density more than 2600 kg/m^3 is understood, although this value is relatively small. Practically, concrete used for shielding purposes has volumetric mass of about 3000 up to even more than 6000 kg/m^3.

To reach a required and reasonable level of density of the concrete, a heavy aggregate or an addition in form of another heavy elements must be contained in the mixture.

Very commonly used as a heavy concrete aggregate is baryte (baryte concrete has volumetric mass up to 4200 kg/m^3). Or it can be limonite, hematite, magnetite, ilmenite etc. To make a denser concrete, the aggregate can be replaced (or more often added) by a cast-iron scrap or pieces of "chopped" iron that can be a by-product from a steel production. These concretes, with an addition of iron/steel, have a significantly high volumetric mass, but they are very badly workable. Interestingly, depleted uranium is sometimes used as well for its high density. Volumetric mass of concrete padded with such aggregate reaches values around 6400 kg/m^3.

Operating conditions of a nuclear power plant present another requirement of the designed concrete and it is resistance to the operating temperature, which reaches values of hundreds. Hence, more chemically bound water is required. Frequently used for shielding structures in nuclear power plants are **serpentinite** (for its high water content and resistance to high temperatures) and **borate** (for its convenient cross-section) [5]. Serpentinite contains relatively lots of chemically bound water and is capable to preserve it to temperatures as high as 450°C. Unfortunately, this follows fairly low density of the concrete (about 2100 kg/m^3), thus the requirement of the higher volumetric mass is not met and more additions are needed - heavier aggregate fractions or cast-iron scrap. Borate (especially boron's isotope ^{10}B), on the other hand, has a significant nuclear cross-section, providing reliable ability to capture slowed or thermal neutron with relatively low emission of secondary radiation. Boron in concrete is usually designed as an addition.

2.2.1 Effect of the radiation on concrete

Effects of radiation on concrete has been studied for over 60 years with uncertain conclusions, mainly due to the difficulty of separating the effect of all the aspects of aggressive environment - gamma radiation, neutron radiation, high

operating temperature and humidity. The complexity of the concrete mixture represents another obstacle given the fact that conclusions of experiments differ, mentioning the influence of concrete composition [3, 4].

Neutron irradiation may cause a damage of crystal lattice structure after collision of a neutron with a nucleus of the shielding material. An atom can be "blasted out" of the lattice, the missing site of the lattice is called vacancy (hence, the vacancy defect), which can eventually cause embrittlement of the material and eventually can lead to breaking the atomic bonds. According to [6], more common defect of the crystal lattice of irradiated concrete is the interstitial defect, which describes a situation where an atom occupies a site in the lattice in which an atom should not be. This results in expansion of the lattice and eventually, expansion of the whole material - in the context of concrete, this takes place in aggregates. Minerals, components of aggregates, expand, creating stress within the structure. As the composition of individual aggregates, naturally, varies from grain to grain, these stresses are not uniform. This mechanism is called **radiation-induced volumetric expansion** (or **RIVE**), which is the primary effect that cause degradation of irradiated concrete [2, 7]. Therefore, aggregates are the most affected by neutron radiation.

These microscopic effects cumulate and lead to the macroscopic change of the material properties. Mentioning concrete, the change of its main characteristics - compressive strength, Young's modulus of elasticity or tensile strength. An important level of neutron irradiation is the fluence of $1 \cdot 10^{19}\, n/cm^2$ (e.g. with VVER 440/213, this value is reached after $\approx$ 10 years of exposure - see Fig. 3.6). After this level, the properties begin to decrease, degrading the concrete, and RIVE starts to represent significant importance. The driving aspects of RIVE value are neutron fluence, temperature and, instinctively, mineral composition of the aggregate. Following pictures (Fig. 2.4, Fig. 2.5 and Fig. 2.6) [7] demonstrate the trend of how the concrete properties are affected by neutron fluence exposure. Fig. 2.7 [7] then shows the dimension change of aggregates due to RIVE.

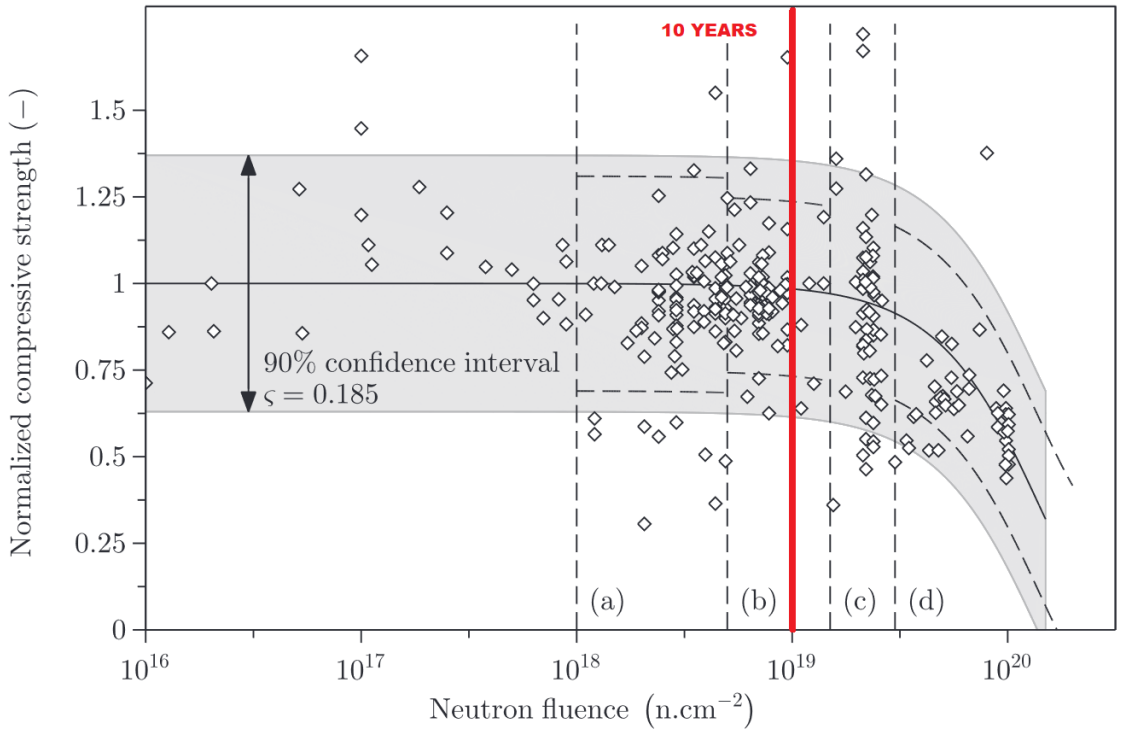

Figure 2.4: Compressive strength decrease depending on the neutron fluence

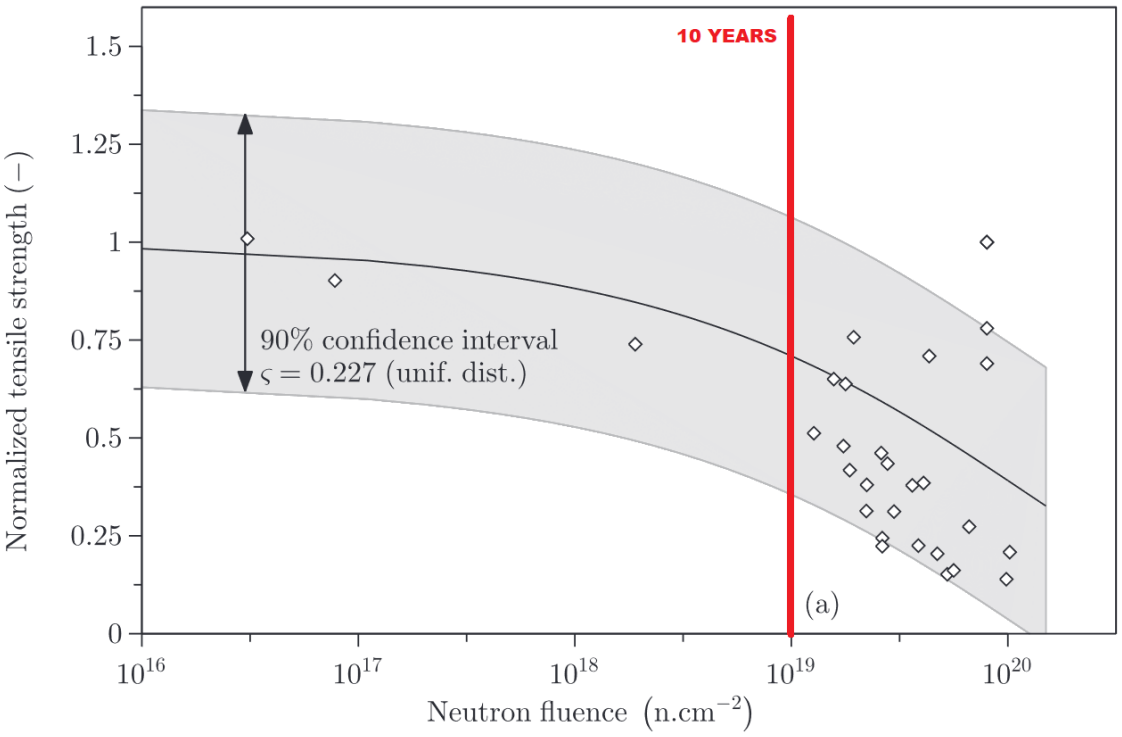

Figure 2.5: Tensile strength decrease depending on the neutron fluence

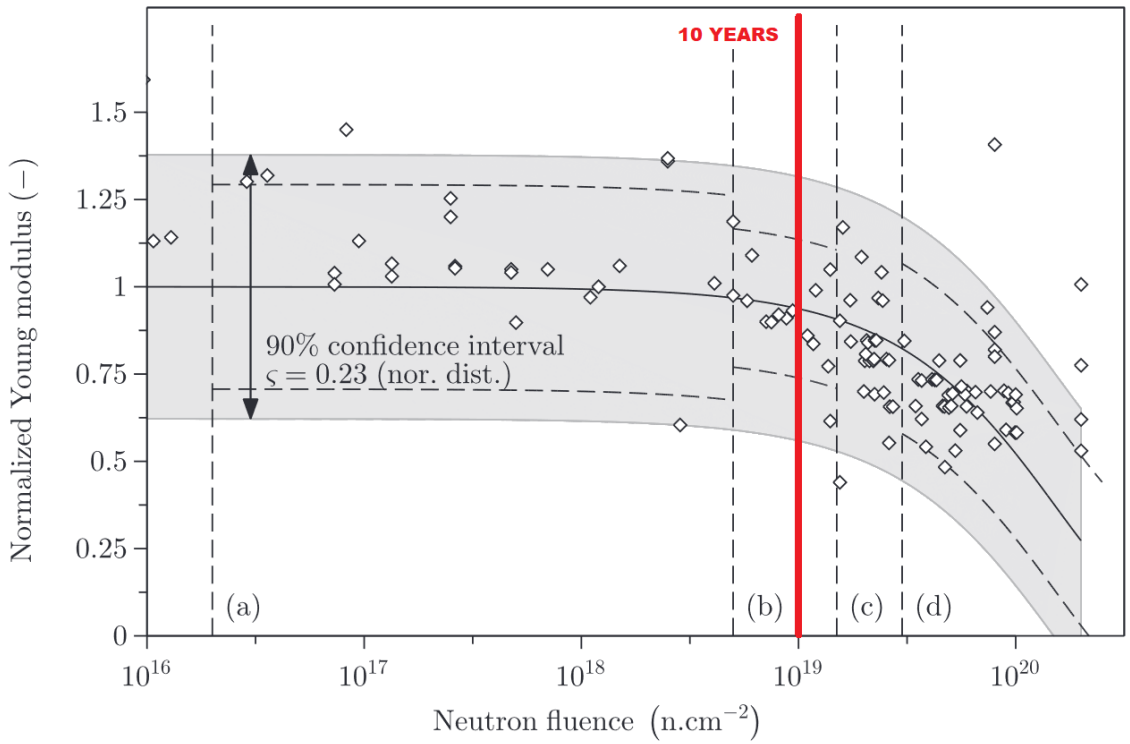

Figure 2.6: Young's modulus of elasticity decrease depending on the neutron fluence

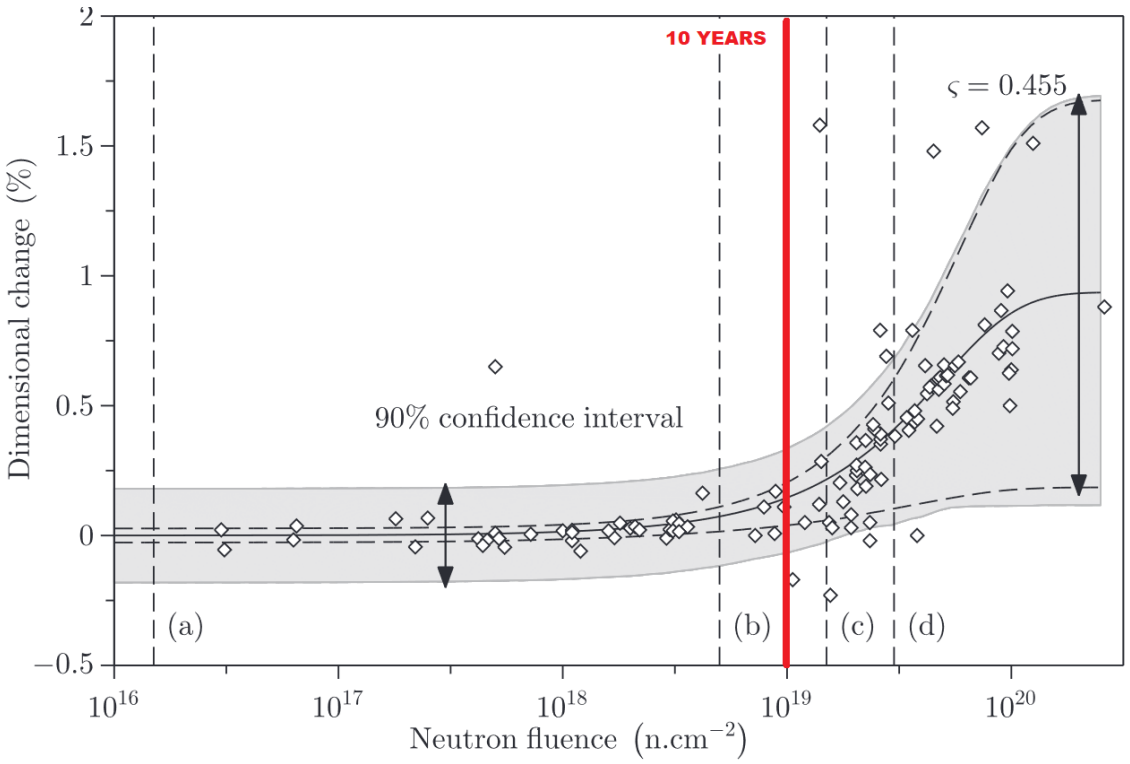

Figure 2.7: Dimensional change of aggregates (RIVE) depending on the neutron fluence

Gamma radiation does not affect aggregates as much as neutron radiation, but rather affects the cement paste via heating and radiolysis of porous water content, resulting in risks of internal overpressure within the cement matrix, increasing the hydrogen gas generation, carbonation and drying [8, 9]. Multiple studies [3, 9] agree on that the effect of long term exposure to γ radiation does not present a significant problem that would need to be taken into account when designing the shielding structure and that it would affect mechanical properties, only the effect of heating and drying should be counted in. The study [10] shows results of experiment that proved low to none effect of γ radiation on compressive strength of the cement paste. And the study [9] even claims that cement paste that undergoes γ irradiation has increased strength due to γ-ray-induced carbonation and formation of vaterite mineral.

CHAPTER 3

Numerical analysis of a Concrete Biological Shield

Main part of the work was to create a finite-element method program. Numerical model for analysis of a concrete biological shield of a nuclear reactor VVER 440/213 was created using computing software MATLAB. This chapter describes the considered model and made assumptions, explains steps of assembling stiffness matrix and applying load. Last but not least, introduces methods implemented in the program to conduct a non-linear part of analysis, describing non-linear behaviour of concrete.

Concrete biological shield (CBS) is a ring-shaped structure around the nuclear reactor's active zone (Fig. 3.1 - the right picture shows older type VVER 440/230 that had a biological shield in the form of water tanks) designed to shield radiation resulting from the nuclear fission in the reactor. There are many types of these structures, varying basically with every nuclear power plant construction. Overall, these structures are mostly a regular cylinder of various thickness, ranging from ≈ 0.7 up to ≈ 2 m. From view of the load of the CBS, two types can be distinguished: self-bearing CBS that only serves the purpose of shielding and the load besides radiation is only its self-weight, the other case is that the CBS is not just for shielding, but its purpose is also providing support to the reactor

pressure vessel. If the CBS is a supporting structure, the requirements are even more strict and the capability of long term load capacity and limit displacements have to be designed with taking the long term effects of radiation into account.

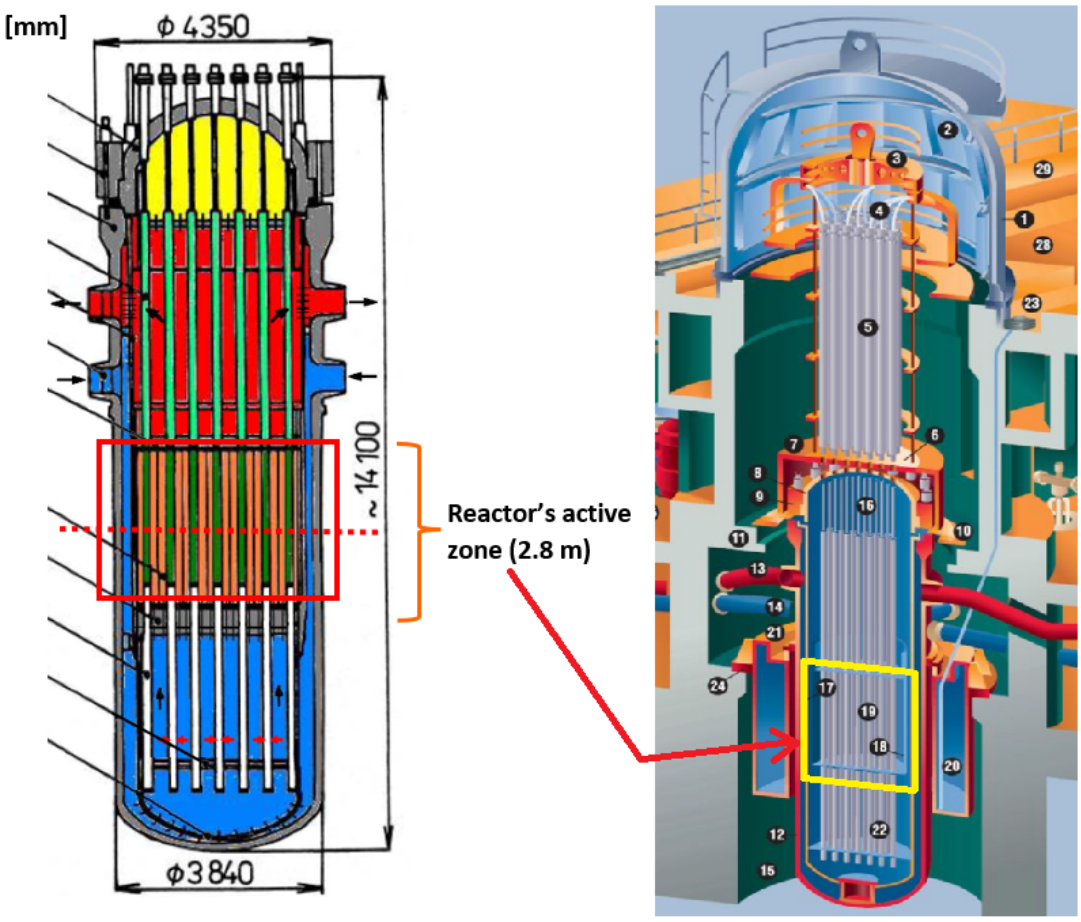

Figure 3.1: Schematic vertical sections of reactors VVER 440 with highlighted active zone

3.1 Geometry and model description

The concrete biological shield structure considered in this particular analysis corresponds to the CBS of a reactor VVER 440/213, which is a type originating in 1970s, but is very common in European NPPs as of today (e.g. Czech NPP Dukovany consists of only these reactors). The CBS is a cylinder-like structure with trapezoidal cross-section of height 2.8 m, maximum thickness 0.7 m and inner radius 2.37 m. These dimensions correspond to the CBS of VVER-440/213 (see Fig. 3.2 [11] and Fig. 3.3) [11].

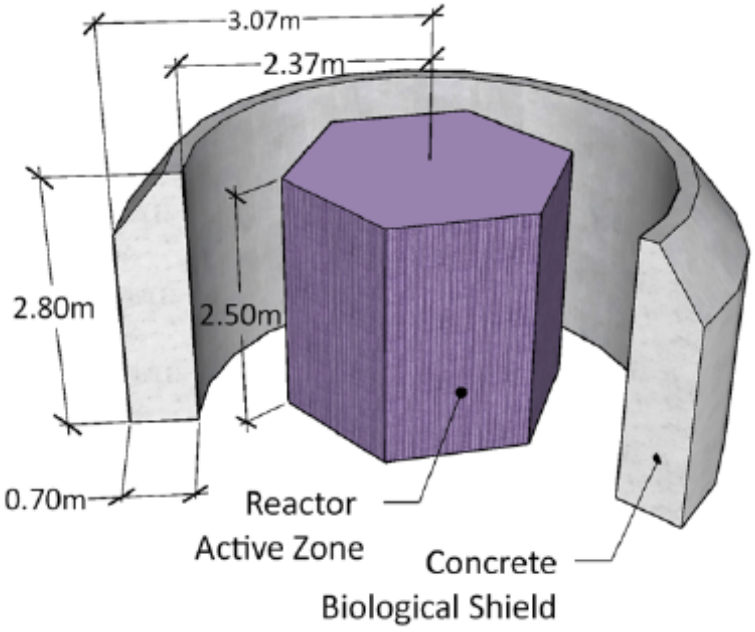

Figure 3.2: Geometry of the considered VVER 440/213 concrete biological shield - axonometry

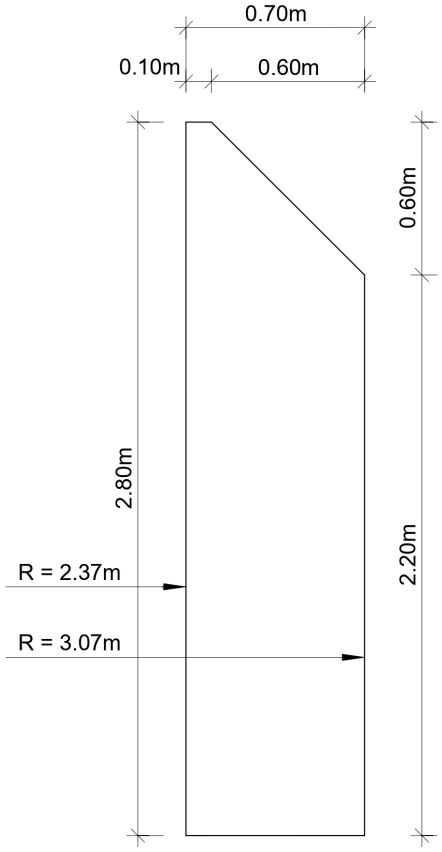

Figure 3.3: Geometry of the considered VVER 440/213 concrete biological shield - cross-section

As for material, the concrete structure is considered homogeneous without reinforcement. Closer look in Chapter 3.5.3 in Table 3.1.

The analysis was performed by finite element method with a discretization into two-dimensional regular mesh of right-angled triangles (the structure consists of a total of 5696 elements and 2977 nodes). Size of the triangles were adapted from the virtual compression test (described later in Chapter 3.5.3) with an intention to decrease mesh dependency. Triangles with length of the legs 0.025 m were used, later on changed to 0.05 m to inspect the mesh dependency (more in Chapter 4). First, the borderlines shaping a rectangular cross-section were defined by points with the distance of 0.025 m. These points were copied in both directions, again by the distance of 0.025 m. The result was a rectangular field of evenly distributed points. All points lying outside of the geometry (ergo points in the upper right corner) were eliminated. Then, the triangular mesh was generated using the Delaunay triangulation method. This method connects given set of nodes in triangles by the rule that inside no circumcircle of any triangle lies any node (discretization can be seen in Fig. 3.4).

The CBS structure is assumed as an axisymmetric structure. Axisymmetric solid body is defined as a three-dimensional body generated by rotating a cross-section around an axis of symmetry. Besides geometry, support conditions, loads and material properties must all meet the axisymmetric requirements (equal in every single section of the structure) [12]. Thus, the finite elements are better described as solid ring-shaped elements with triangular cross-section. In this case, the axis of symmetry is called z and the radial direction is called r with the origin being the point where the symmetry axis intersects the plane given by the bottom of the CBS structure. For the purposes of later description, the third direction (perpendicular to the rz *plane*) is referred to as *circumferential*.

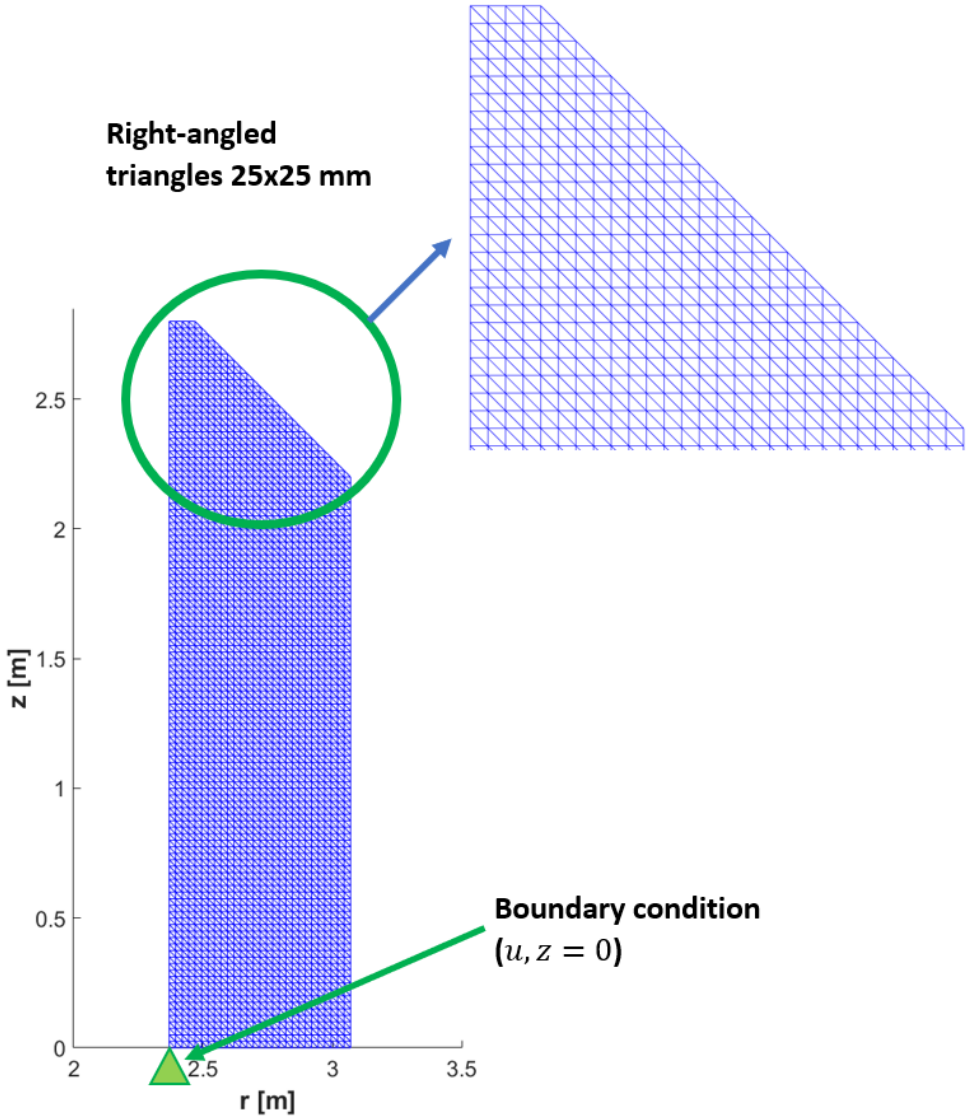

Figure 3.4: Geometry and triangular mesh generated in MATLAB

As for the boundary conditions (BC), both degrees of freedom are restricted ($u_r = u_z = 0$) in the left-most bottom corner node (marked by a green triangle in Fig. 3.4). As far as axisymmetry represents a "semi-3D" model, the third restriction (in the circumferential direction) is represented by a spatial stiffness of the ring-like structure. To liken the BC to reality, the bottom-left node represents a fixed connection of the CBS with the inner steel liner by welding.

3.2 Calculation

A structure with boundary conditions that restrict movement of the structure as a rigid body deforms according to the principle of the minimum potential energy. This means that every constrained system, after applying load, will get to the state of deformation that need the least energy to get to. In other words, according to the potential energy principle, that configuration which satisfies the boundary condition corresponding to equilibrium state will make the total potential energy a minimum [13].

This fact, the equilibrium is represented by equation Eq. 3.1 (or rather system of linear equations), which states the equilibrium between internal and external forces as a result of Ritz-Galerkin method [14]. Linear shape functions were used to approximate solution. Solving this system of equations is a crucial part of the finite element analysis.

$$\mathbf{K}\,\mathbf{u} = \mathbf{f}, \tag{3.1}$$

where $\mathbf{K}$ stands for the global stiffness matrix, $\mathbf{u}$ is a column vector of unknown variables (displacements) and $\mathbf{f}$ is vector of the external forces. Assembly of the global stiffness matrix and creating the vector of forces are closer described in following sections. Vector of unknowns $\mathbf{u}$ is of dimension 5954x1 (2*nodes) and consists of the displacements of DoF (e.g. u_1 is the the first node's r displacement, u_2 is first node's z displacement, u_3 second node's r displacement etc.).

The boundary conditions defined for given structures are assumed at the left-bottom node of the section (where $z = 0$ m and $r = 0 + radius$). Both displacements, vertical and horizontal, are prescribed to be equal zero.

There are two methods to apply boundary conditions in calculations; these are *Elimination approach* and *Penalty method*. The penalty method is more general, its application is particularly useful in models with imperfectly flexible supports (or supports with a particular stiffness) [15].

In the created program, the elimination approach was used. First step of this method is saving the code numbers corresponding to the desired boundary conditions and then, when solving the system of equations, rows respecting the saved code number are excluded from the process (as for stiffness matrix, both rows and columns corresponding to the saved code number are excluded). Next step is the solution of the main unknowns (vector of displacements **u**) itself. To solve the equations system, the *Gauss Elimination* method is applied. After obtaining the solution, linear deformation and stresses of individual elements can be calculated with Eq. 3.2 and Eq. 3.3.

Vector of deformation equals to the vector of, now known, nodal displacements multiplied by the matrix of shape functions **B** (more precisely their derivations) for axisymmetric problem (more detailed description in the following section). Components of this vector consists of deformations in the separate directions r, z, *cir* and *shear* respectively. As far as the calculation is still linear, vector of stresses is obtained by multiplying the stresses by the material matrix **D** (closer specification in next section). Components of this vector are, similarly, stresses in the separate directions.

$$\boldsymbol{\varepsilon} = \mathbf{B}\,\mathbf{u} \longrightarrow \boldsymbol{\varepsilon} = \begin{pmatrix} \varepsilon_r \\ \varepsilon_z \\ \varepsilon_{cir} \\ \gamma_{rz} \end{pmatrix} \tag{3.2}$$

$$\boldsymbol{\sigma} = \mathbf{D}\,\mathbf{B}\,\mathbf{u} = \mathbf{D}\,\boldsymbol{\varepsilon} \longrightarrow \boldsymbol{\sigma} = \begin{pmatrix} \sigma_r \\ \sigma_z \\ \sigma_{cir} \\ \tau_{rz} \end{pmatrix} \tag{3.3}$$

3.3 Assembling global stiffness matrix

Every node has two degrees of freedom, vertical and horizontal displacement. Each degree of freedom is represented by a unique global code number. Therefore, in this case, there are two code numbers for every node. Assigning code numbers to the nodes is an important step as it declares dimensions of the load and displacement vectors as well as the global stiffness matrix, basically establishing the local-global relationship.

Stiffness matrices are assembled separately for every individual element with local code number (for triangles with two DoF in each vertex local code numbers are $1-6$). These partial matrices are then localized using given global code numbers into the global stiffness matrix of the structure. This method is called direct stiffness method or the direct approach.

$$\mathbf{K} = \sum_{e=1}^{n} \mathbf{k}^{(e)}, \tag{3.4}$$

where $\mathbf{k}^e$ is a partial stiffness matrix (local stiffness matrix) of an eth element and $\mathbf{K}$ is the global stiffness matrix. The formula for axisymmetric element stiffness matrix is derived from minimum of potential energy, minimization uses Rayleigh-Ritz method [15]:

$$\mathbf{k} = \int_{\Omega} \mathbf{B}^T\mathbf{D}\mathbf{B}d\Omega = 2\bar{r}\int_{A} \mathbf{B}^T\mathbf{D}\mathbf{B}dA = 2\bar{r}\mathbf{B}^T\mathbf{D}\mathbf{B}\int dA \tag{3.5}$$

$\mathbf{B}$ is a matrix containing the shaping functions (more precisely derivatives of these functions). The shape functions are linear, therefore the $\mathbf{B}$ matrix, consisting of their derivations, is constant. $\mathbf{D}$ is a material matrix, also a constant, where two material parameters appear, Young's modulus of elasticity and the Poisson's ratio. All constants can be moved outside the integral and the result is given formula for matrix of eth finite element:

$$\mathbf{k}^{(e)} = 2\pi\bar{r}A_e\mathbf{B}_e^T\mathbf{D}_e\mathbf{B}_e, \tag{3.6}$$

Matrix of the derivatives of the shape functions for axisymmetric problem [12]:

$$\mathbf{B}_e = \begin{bmatrix} \beta_i & 0 & \beta_j & 0 & \beta_m & 0 \\ 0 & \gamma_i & 0 & \gamma_j & 0 & \gamma_m \\ \frac{\alpha_i}{\bar{r}} + \beta_i + \frac{\gamma_i \bar{z}}{\bar{r}} & 0 & \frac{\alpha_j}{\bar{r}} + \beta_j + \frac{\gamma_j \bar{z}}{\bar{r}} & 0 & \frac{\alpha_m}{\bar{r}} + \beta_m + \frac{\gamma_m \bar{z}}{\bar{r}} & 0 \\ \beta_i & \gamma_i & \beta_j & \gamma_j & \beta_m & \gamma_m \end{bmatrix}$$

α, β and γ are values depending on the size and orientation of the given element, they represents value of the derivatives of the shape functions in individual vertices of an element. $\bar{r}$ and $\bar{z}$ are coordinates of the center of mass of the elements.

$$\alpha_i = r_j z_m - z_j r_m \qquad \beta_i = z_j - z_m \qquad \gamma_i = r_m - r_j$$

$$\alpha_j = r_m z_i - z_m r_i \qquad \beta_j = z_m - z_i \qquad \gamma_j = r_i - r_m$$

$$\alpha_m = r_i z_j - z_i r_j \qquad \beta_m = z_i - z_j \qquad \gamma_m = r_j - r_i$$

$$\bar{r} = \frac{r_i + r_j + r_m}{3} \qquad \bar{z} = \frac{z_i + z_j + z_m}{3}$$

The lower indices (i, j, m) to the variables r and z refer to the nodes of the given element as shown in the picture (Fig. 3.5). This corresponds to the connectivity order of vertices of each element.

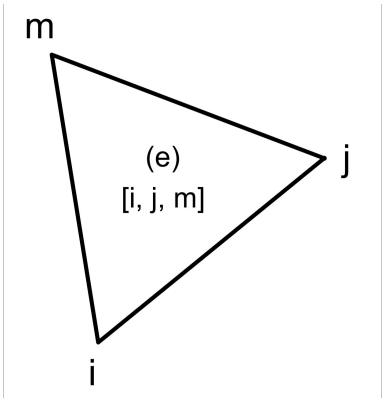

Figure 3.5: A general triangle representing order of code numbers of an element

The material matrix in case of axisymmetric body is:

$$\mathbf{D}_e = \frac{E}{(1+\nu)(1-2\nu)} \begin{bmatrix} 1-\nu & \nu & \nu & 0 \\ \nu & 1-\nu & \nu & 0 \\ \nu & \nu & 1-\nu & 0 \\ 0 & 0 & 0 & \frac{1-2\nu}{2} \end{bmatrix}$$

where E stands for Young's modulus of elasticity and ν is Poisson's ratio (specified in Chapter 3.5.3 in Table 3.1).

Each vertex of every triangular finite element has two DoF, vertical and horizontal displacement. Therefore, the dimension of a stiffness matrix of one element is $6x6$ $(2 * nodes)$. in the case of given CBS structure, there is total of 2977 nodes, thus the dimension of global stiffness matrix is 5954 x 5954.

3.4 Applied load

Considered concrete biological shield is a self-bearing structure, therefore, it supports only its mass weight and the primary load presents the environment - the radiation, moisture and temperature. As was stated earlier in chapter (Chapter 2.2), gamma and neutron radiation must be taken into account in a CBS analysis. Gamma radiation affects mostly the cement mortar, so it reflects in reduction of concrete properties (this phenomenon is not included in the program). The neutron radiation, on the other hand, has a significant effect - RIVE (explained with more details in Chapter 2.2.1 and has to be projected into calculation in the first place [7]).

Two types of load are considered in the created program: self weight and RIVE.

The load is applied in separate steps corresponding to years of operation of the reactor or the CBS time exposure to the radiation (step 1 - one-year neutron fluence, step 2 - two-year neutron fluence, etc). In every step, the full load is applied separately and the total displacement calculated without modifying the stiffness matrix. Two check-ups are executed in the loading steps;

first, the principal strain is evaluated to the strain from the previous step, if it is of a smaller value, the value from the previous step is accepted. The same approach is applied after damage determination, which is evaluated likewise. Both evaluations are conducted due to the logical fact that once a deformation or damage occur, the material cannot return to the undamaged state (essentially, if a crack of a certain size appears, it cannot "heal" itself again and recover the concrete properties). Although this is computationally more expensive - more time to converge as the initial solution is further from the exact one compared to the calculation of only the increments of displacement caused by increments of the load applied. Despite this fact, the solution converges to the same value in both approaches.

Firstly, the self weight is implemented fairly simply. The body force per unit volume is constant for all elements. However, each elements is evaluated to the axis of symmetry in the direction of r, therefore, every element has a different vector of the force of gravity. The force is calculated for the center of gravity (CG) and evenly divided into three vertices of the element (assigned to the appropriate position of the force vector using code numbers).

$$f_{CG}^{(e)} = -2\pi A_{(e)} \bar{r} \rho \quad \longrightarrow \quad \mathbf{f}^{(e)} = \frac{1}{3} \begin{Bmatrix} 0 \\ f_{CG}^{(e)} \\ 0 \\ f_{CG}^{(e)} \\ 0 \\ f_{CG}^{(e)} \end{Bmatrix}, \tag{3.7}$$

where $f_{CG}^{(e)}$ is the force of self weight in the CG of an eth element, $A_{(e)}$ is the area of the element, $\bar{r}$ is the r coordinate of the CG and ρ stands for body force per unit volume (in the program, the value of $\rho = 40\ kN/m^3$ is considered - a concrete with density of $4000\ kg/m^3$). And finally, $\mathbf{f}^{(e)}$ is the particular force vector for the element, which is then localized to the global vector by code numbers.

The more important part of the applied load is RIVE. As the name suggests, it is a volumetric change, therefore it steps into the calculation in the form of homogeneous strain ε_{RIVE}, which represents expansion of the whole elements. It is then distributed in strains in all three directions (approximated that it expands evenly by 1/3 in every direction):

$$\varepsilon_r = \varepsilon_z = \varepsilon_{cir} = \frac{1}{3}\,\varepsilon_{RIVE} \tag{3.8}$$

The RIVE strain is driven by neutron fluence and is modeled by Zubov's function modified by Y. Le Pape [7] based on experimental data:

$$\varepsilon_{RIVE} = \kappa\varepsilon_{max}\frac{e^{\delta\Phi} - 1}{\varepsilon_{max} + \kappa e^{\delta\Phi}} \tag{3.9}$$

where ε_{RIVE} is the strain caused by RIVE, κ a parameter homogeneous to strain, ε_{max} is a maximum expansion, δ stands for inverse fluence and Φ is the neutron fluence. Following values of the parameters were considered in the program to best describe the function according to Y. Le Pape [7]: $\kappa = 0.00968$, $\varepsilon_{max} = 0.00936$, $\delta = 3.092 \cdot 10^{-20}\ cm^2/n$.

The neutron fluence Φ is specified by multiple parameters illustrated by the following figure (see Fig. 3.6).

The picture Fig. 3.6 shows distribution of neutron fluence along the height of the shielding structure on its inner surface. The range maximum values of the functions correspond to the height of the center of the reactor's active zone. These data are obtained by lowering a detector into the active zone, recording the frequency of impulses (captured neutrons) per a unit of time.

The real fluence is not of the same value over the whole circumference, but rather corresponds to the active zone's hexagonal shape of horizontal section (see Fig. 3.7a [16]). However, this fact does not allow usage of axisymmetric analysis. To satisfy the assumption of axisymmetry, the circumferential distribution was averaged to be of the same value in every point (see Fig. 3.7b [11]).

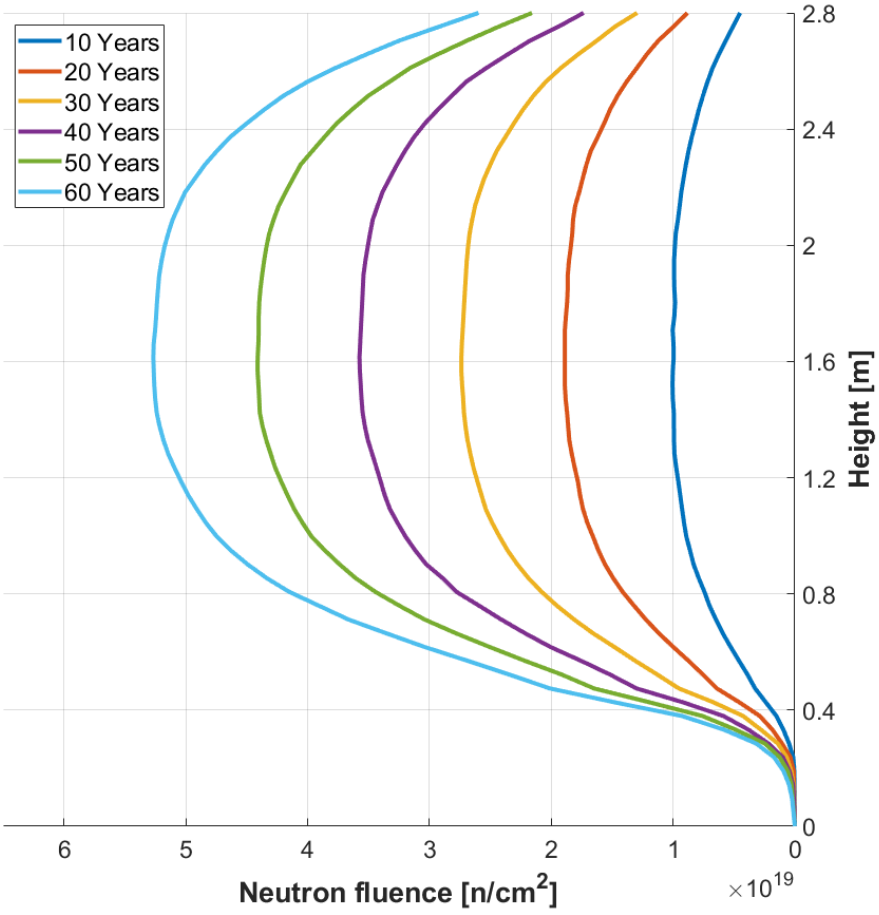

Figure 3.6: Neutron fluence distribution along the height in 10/20/.../60 years

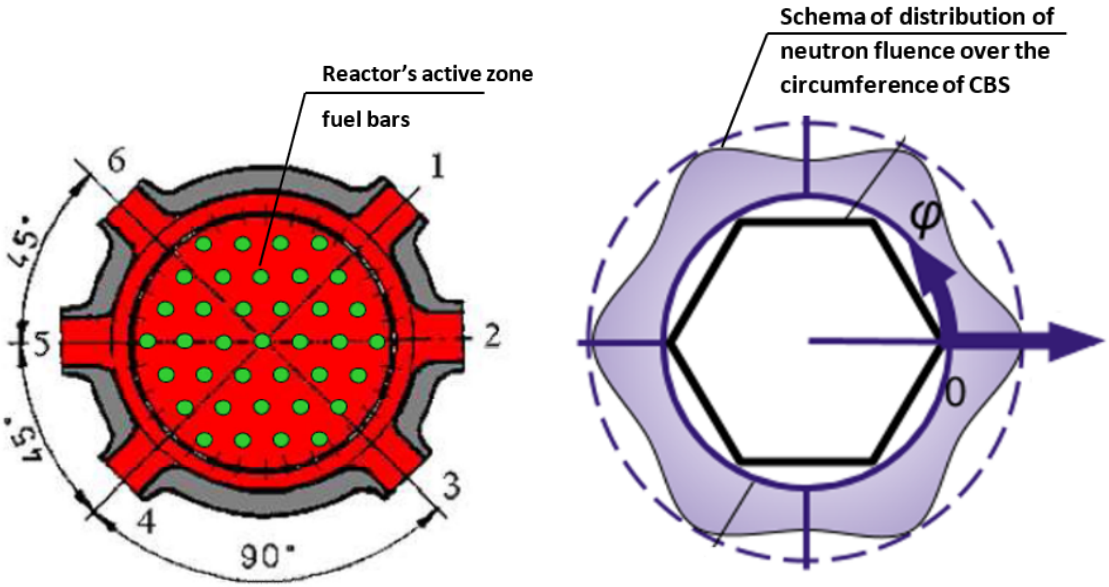

(a) Schema of horizontal section of the VVER 440/213

(b) Schema of fluence distribution over the inner circumference of the CBS

Figure 3.7: Real distribution of fluence over the circumference of CBS

Next picture (Fig. 3.8) points out the fact that the fluence does vary along height as well as it depends on the depth due to the effect of shielding, which is called *attenuation*. It results in a different value of fluence at any point of the section. Therefore, regarding FE analysis, different load by RIVE must be applied on different finite elements.

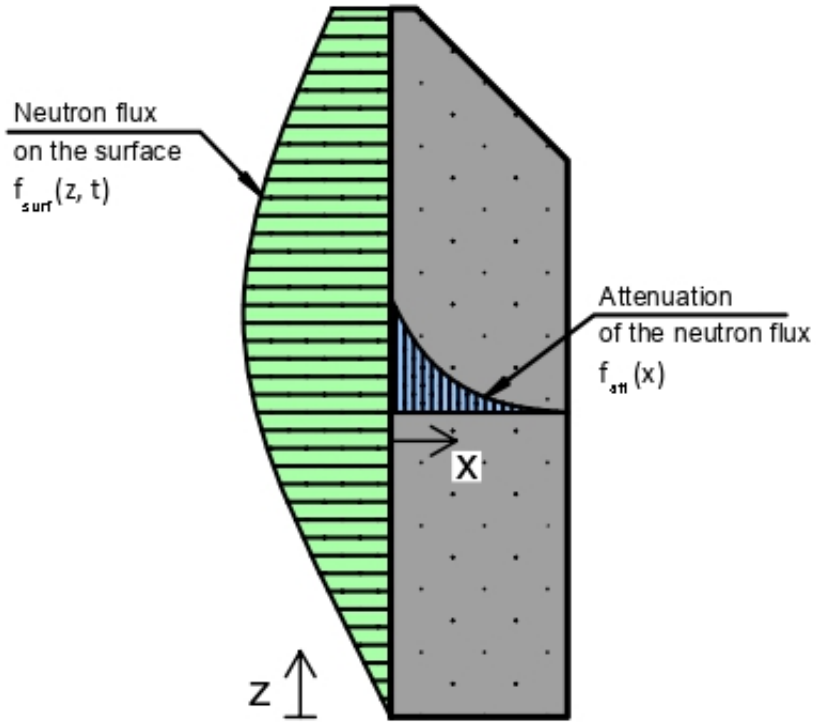

Figure 3.8: Schema of Neutron flux distribution along the height and depth of the cross-section (courses of the functions are only illustrative)

The function of the flux attenuation is described by following relation (according to [17] and [18]):

$$f_{att} = f(x) \tag{3.10}$$

$$f_{att} = f_{surf} \cdot e^{-\sum_R x}, \tag{3.11}$$

where f_{att} is the neutron flux at the particular point of the structure (or in a particular element), f_{surf} is the neutron flux on the inner surface of the structure obtained from the graphs in the Fig. 3.6, $-\sum_R$ denotes the effective removal

cross-section of the neutrons that states the probability with which a neutron will collide with a target nucleus. And at last, x stands for the depth into the structure, the driving variable of the f_{att} function. The following picture (Fig. 3.9) shows the effect of attenuation. It is clear that the attenuation has significant impact on the total neutron fluence. In the depth of $\approx$ 120 mm, the attenuated ratio of fluence decreases below 0.1. This can be seen also in the next picture (Fig. 3.10), where the highest values of strain caused by RIVE is in the layer of inner surface and decreases vigorously. The strain distribution in the figure also shows that its shape corresponds to the graphs in Fig. 3.6.

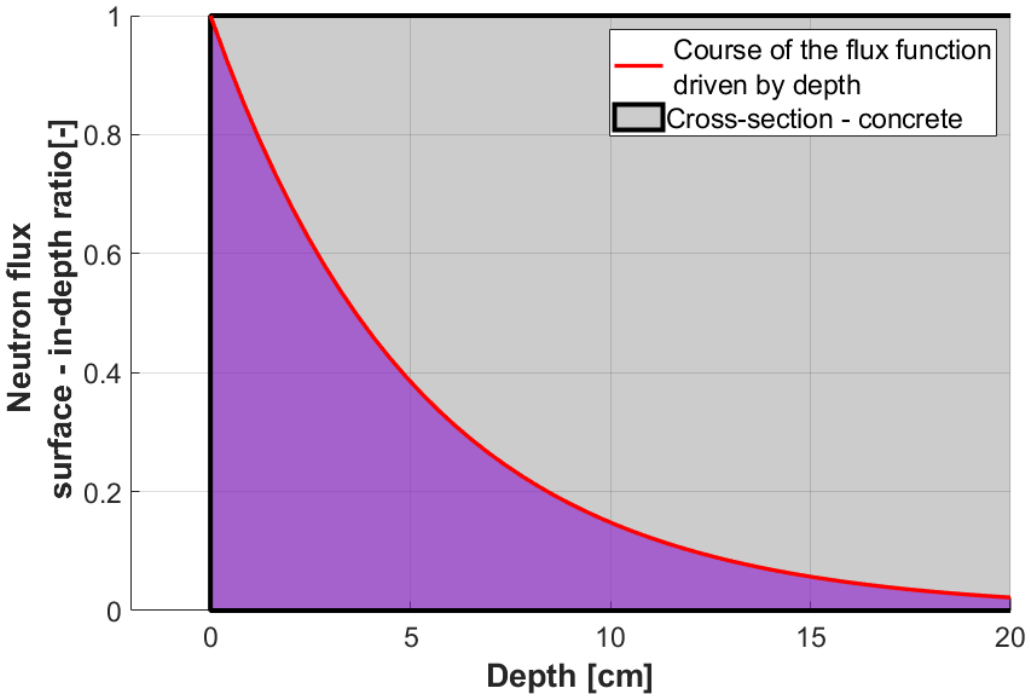

Figure 3.9: Course of Attenuation of the neutron flux function driven by the depth variable

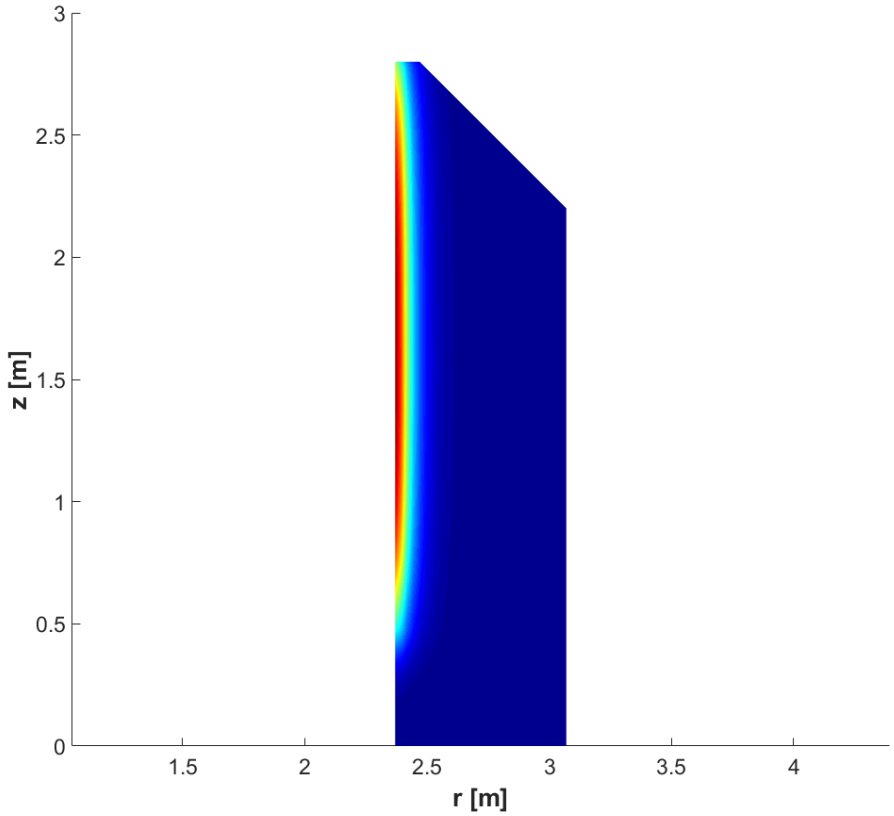

Figure 3.10: Distribution of ε_{RIVE} over the cross-section

3.5 Nonlinear part of the analysis

When a structure represents a body of significant rigidity, applied load is not peculiar or the resulting displacement are not very significant, linear analysis is usually sufficient and its solution provides approximation that is not far from the exact solution. As was discussed in Chapter 2.2, importance of the CBS structure requires higher level of precision as formation of cracks indicate an unreliable shielding capability. On top of it, the primary goal of the analysis is to determine the origin and eventually the development of damage (cracking). An important role while considering using nonlinear analysis is its purpose and level of precision. Therefore, in the case of CBS, the nonlinear model is essential.

Concrete is a material well known for its nonlinear behaviour, then the material nonlinearity needs to be taken into account. Nonlinear behaviour occurs upon

reaching a certain level of stress, mentioning concrete, this level is called a *threshold of damage*. Microcracks are starting to form and in these spots, the concrete structure is not capable of resisting the stress. At this point, the linear relationship between load and response (displacement, stress, strain) cannot be accounted for anymore.

In general, most of the methods, if not all, used for solving nonlinear problem are iterative. In summary, these methods are all based on linearization of the problem. First, an initial estimate is considered which is then updated during every iteration by a linearly calculated increment, until the required tolerance is reached (tolerance relates to the difference between updated solution and the exact solution). More detailed description of the method used in this algorithm can be found in the next section (Chapter 3.5.1).

3.5.1 Modified Newton-Raphson method

Newton-Raphson is a widely used method for finding roots of nonlinear equations. In the created program, the modified Newton-Raphson method was implemented. The difference between these two methods lies within the usage of the stiffness matrix. Newton-Raphson method builds a new stiffness matrix in every iteration (updates the one from previous iteration and updating it based on the obtained increment Δu), while the modified method works with the initial stiffness matrix in all iteration [19].

In the Fig. 3.11 [19] can be clearly seen the differences between these methods. A system with one degree of freedom is considered. Fig. 3.11 illustrates how updating the stiffness matrix affects the amount of iterations before convergence. In this case, the unmodified method (Fig. 3.11a) converges to the exact solution in just two iterations while the same system solved using the modified method (Fig. 3.11b), the calculation need much more iterations to converge.

As was mentioned above, the key step is estimating the initial value u_0. If the initial estimate were too far from the exact solution, the method would

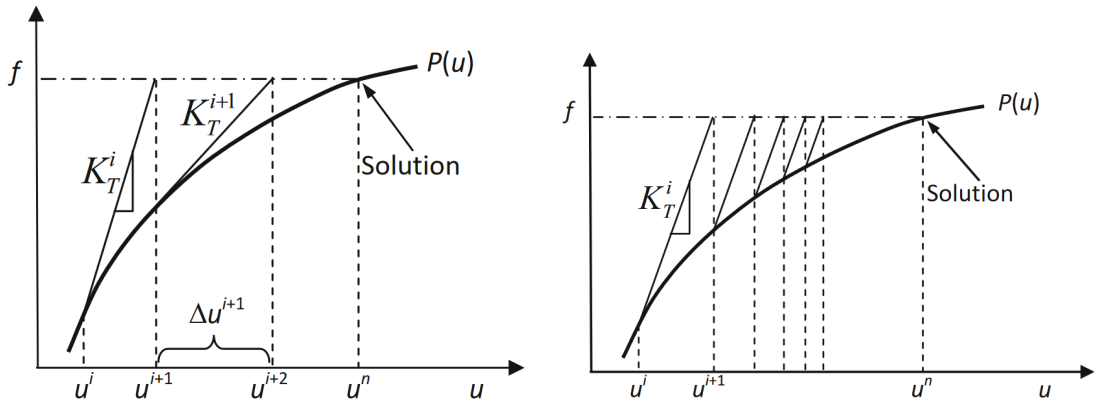

(a) Newton-Raphson method (b) Modified Newton-Raphson method

Figure 3.11: Newton-Raphson and Modified Newton-Raphson methods comparison

never converge, quite the contrary, the solution would be diverging further from the exact solution with each iteration. The solution of the linear analysis was used as the initial estimation ($u_0 = u_{lin}$) for further calculation. In the first iteration, the initial estimation is updated by adding the increment obtained from solving Eq. 3.13. This process is repeated in every iteration; after calculating the increment, it's added to the solution from previous iteration. Process is stopped after either converging to the correct solution with given tolerance (reaching equilibrium) or exceeding a set maximum number of iterations. Restricting number of iterations is recommended to prevent long computational time in case of divergence. In case of force-control, the tolerance is controlled by displacement difference. If the absolute value of the maximum displacement in current iteration differs from the one in the previous iteration by more than $0.01mm$ (set in this program), the solution is taken as valid and the modified Newton-Raphson process is ended. All steps included in this procedure will be described closer in the following paragraphs.

A nonlinear function $P(u)$ is considered to stand for internal forces. Equilibrium of internal forces and applied load must be reached. Therefore, applying the first degree of Taylor expansion results in following equation approximating

solution of the function in the next iteration [19]:

$$\mathbf{P}(u^{i+1}) \approx \mathbf{P}(u^i) + \mathbf{K}\,\boldsymbol{\Delta}\mathbf{u}^i = \mathbf{f}, \tag{3.12}$$

where i stands for number of current iteration, $\boldsymbol{\Delta}\mathbf{u}$ is the increment of displacement and $\mathbf{f}$ is a vector of applied forces. This results in an equation with $\boldsymbol{\Delta}\mathbf{u}$ remaining as the unknown variable in the system of linear equations.

$$\mathbf{K}\,\boldsymbol{\Delta}\mathbf{u}^i = \mathbf{f} - \mathbf{P}(u^i) \tag{3.13}$$

$$\mathbf{df} = \mathbf{f} - \mathbf{P}(u^i) \tag{3.14}$$

$$\mathbf{K}\,\boldsymbol{\Delta}\mathbf{u}^i = \mathbf{df}^i \tag{3.15}$$

Solving this system of equations provides the increment of displacement. In the program, same as solving the equation Eq. 3.1, the Gaussian elimination method is used. In the next step, the increment is added to the solution from previous iteration. This solution is then used in next iteration as the initial value.

$$\mathbf{u}^{i+1} = \mathbf{u}^i + \boldsymbol{\Delta}\mathbf{u}^i \tag{3.16}$$

The variable **df** mentioned in Eq. 3.14 is called *residuum* and represents difference between applied forces and internal forces. Vector of nonlinear function $\mathbf{P}(u^i)$ (or the internal forces) is determined according to the nonlinear behaviour of concrete described by Mazars' damage model. This part of analysis is presented in the next section (Chapter 3.5.2). In other words, if **df** would be equal to zero, it would mean that the equilibrium has been reached and the solution is exact. The relationship between $\boldsymbol{\Delta}\mathbf{u}$ and **df** is linear, thus the smaller is the value of **df**, the smaller is the increment and the difference between displacements in two consecutive iterations approaches zero. If this increment is smaller than set tolerance, the process stops and the solution is considered correct. Summary of how exactly is the method used in the program is shown in the following figure (Fig. 3.12).

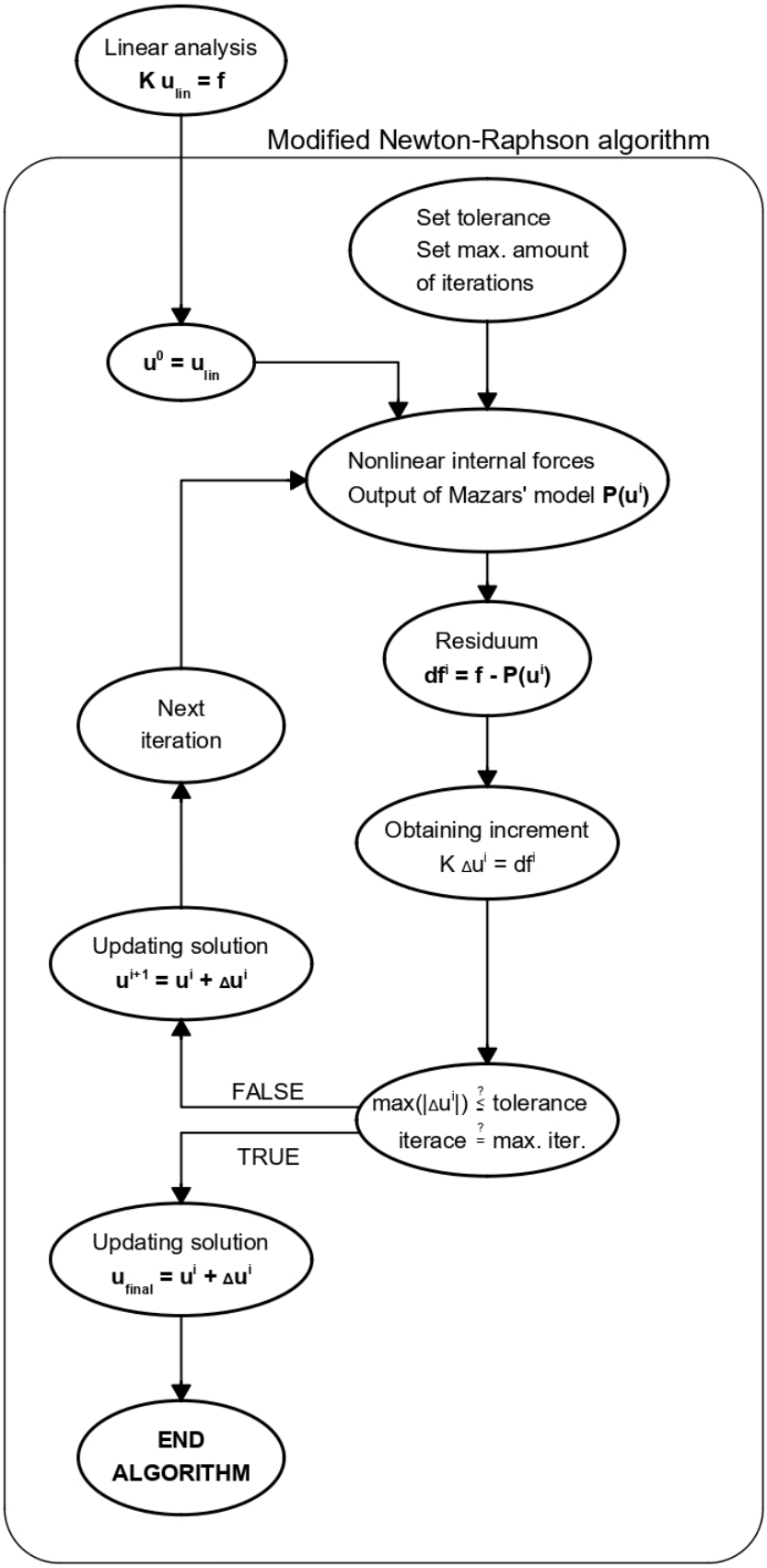

Figure 3.12: Modified Newton-Raphson method flowchart as used in the program

3.5.2 Mazars' μ Damage Model

Mazars' damage model describes nonlinear behavior of concrete and allows conducting a nonlinear analysis (Fig. 3.13). With material such as concrete, the behavior is mainly caused by cracking, which can be basically viewed in two forms - microscopic and macroscopic. In simplified point of view, concrete is a composite of grains of the aggregate and the cement paste. As a load is applied, the grains, due to contact interaction with the cement paste, begin building microcracks around them. The microcracks then spread through the cement matrix causing its disruption and eventually overgrowing into macrocracks that influence performance of the concrete (most importantly its strength properties)[20]. Level of these cracks (damage) is the primary output of the Mazars' model.

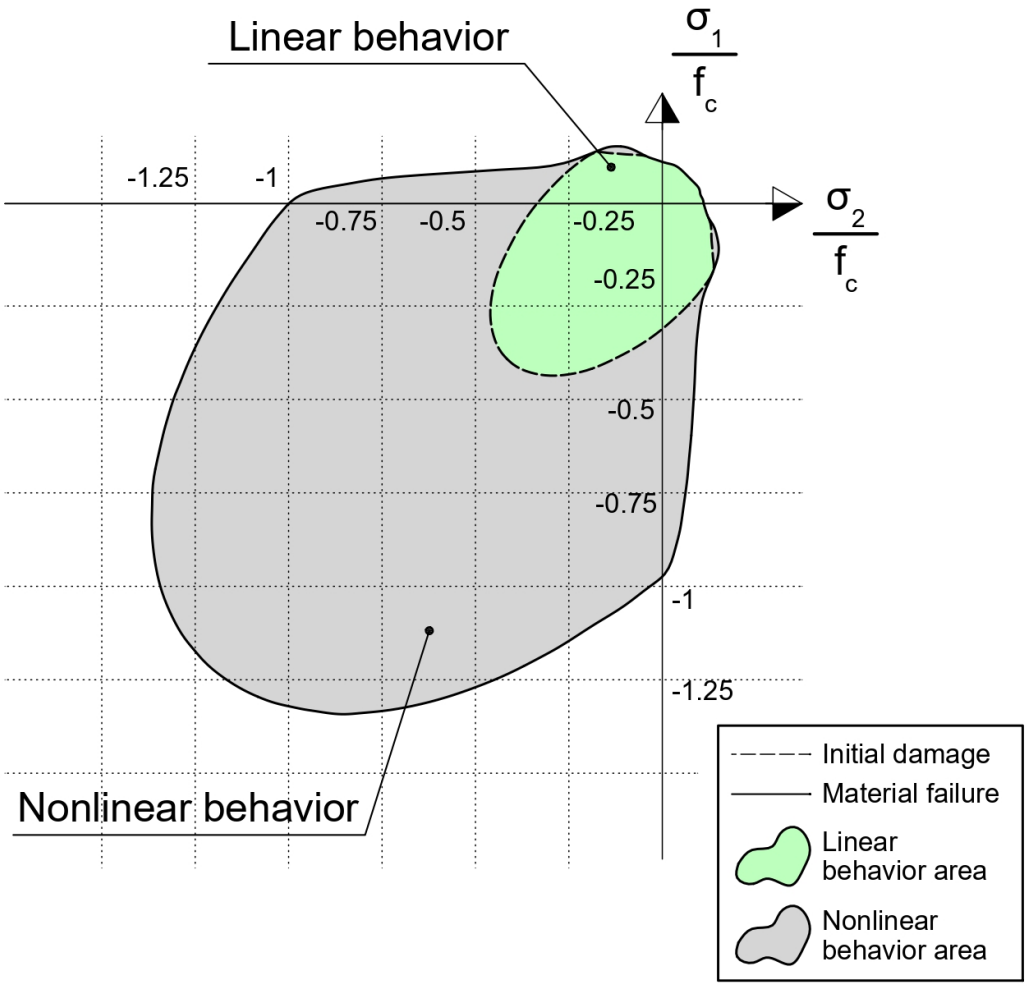

Figure 3.13: Mazars' μ damage model

In this thesis, a 3D model with a local damage approach is considered [21]. This chapter outlines the procedure implemented in the created program. The model needs particular input parameters corresponding to the actual concrete. These parameters are usually fitted on a real experiment. However, in this work, the real experiment was not performed, so the virtual compression test was simulated instead. More information about the test and subsequent fitting parameters is presented in the later section (Chapter 3.5.3).

The stress/strain tensors assembled from the stresses/strains calculated in linear analysis are the main input for the model (or rather the principal stresses/strains). As was stated earlier, the desired output of the model is an isotropic damage variable d for the individual elements. This variable ranges between 0 and 1, indicating intact or fully damaged material, respectively. The damage corresponds to the ability of the element to resist the applied stress.

$$\begin{aligned} d &= f\left(A, B, Y, Y_0\right) \\ \sigma_{damaged} &= (1-d)\sigma, \end{aligned} \tag{3.17}$$

where $\sigma_{damaged}$ stands for the stress of the element taking into account the level of damage and σ is the linearly obtained stress. Damage function d is driven by listed variables; A and B are variables based on parameters identified from compression and flexural tests, adjusting the stress-strain curve (especially the part after reaching the ultimate strength). The damage evolution is defined as follows:

$$d = 1 - \frac{(1-A)Y_0}{Y} - A\, exp(-B(Y - Y_0)), \tag{3.18}$$

This value is checked (more or less only to be sure of the correctness of the calculation), if it is not smaller than the one in last loading step.

$$A = A_t(2r^2(1-2k) - r(1-4k)) + A_c(2r^2 - 3r + 1) \tag{3.19}$$

$$B = r^{r^2-2r+2}B_t + (1 - r^{r^2-2r+2})B_c \tag{3.20}$$

A and B are the variables mentioned above, depending on parameters obtained from results of compression and flexural tests and r is so called triaxial factor that informs about the stress state of an element as can be seen in this relation:

$$r = \frac{\sum_{i=1}^{3} \langle \boldsymbol{\sigma_i} \rangle^+}{\sum_{i=1}^{3} |\boldsymbol{\sigma_i}|}, \tag{3.21}$$

it is a ratio of positive (tensile) stress components (hence the + sign as upper index) and sum of the absolute values of all the principle stresses. Then it is clear that if $r = 1$, the element is in full tension, on contrary, if $r = 0$, the element is compressed in all directions.

Two more variables are mentioned to drive damage evolution, Y and Y_0. The Y takes into account the maximum strain reached during loading path (through the Y_t and Y_c that correspond to the maximum tensile and compression stress domains respectively) and Y_0 brings the initial thresholds into calculation.

$$Y_0 = r\ \varepsilon_{t0} + (1-r)\varepsilon_{c0} \tag{3.22}$$

$$Y = rY_t + (1-r)Y_c \tag{3.23}$$

$$Y_t = max(\varepsilon_{t0}, max(\varepsilon_t)) \tag{3.24}$$

$$Y_c = max(\varepsilon_{c0}, max(\varepsilon_c)) \tag{3.25}$$

The ε_{t0} and ε_{c0} are the initial threshold values described earlier. The exact values used in the program can be seen in the table Table 3.1. The equations Eq. 3.18

and Eq. 3.22 to Eq. 3.25 unequivocally show that if the strains (compressive or tensile) are smaller than the initial thresholds, the damage does not occur (hence $d = 0$) and therefore, the material behaves linearly.

The variables ε_t and ε_c stand for so called *equivalent strain* for cracking and crashing, respectively, calculated as follows [21]:

$$\varepsilon_t = \frac{I_\varepsilon}{2(1-2\nu)} + \frac{\sqrt{J_\varepsilon}}{2(1+\nu)} \tag{3.26}$$

$$\varepsilon_c = \frac{I_\varepsilon}{5(1-2\nu)} + \frac{6\sqrt{J_\varepsilon}}{2(1+\nu)} \tag{3.27}$$

Shown in these relations, both ε_t and ε_c depend on variables I_ε and J_ε, which are the first invariant ($I_\varepsilon = tr(\boldsymbol{\{\varepsilon\}})$) of the strain tensor and the deviatoric part of the tensor respectively [21].

When the real stress in the element $\sigma_{damaged}$ is determined (Eq. 3.17), the nonlinear internal forces can be calculated and passed into the Newton-Raphson algorithm.

$$\mathbf{P} = 2\pi A_e \mathbf{B}_e^T (1-d)\mathbf{D}_e \mathbf{B}_e \mathbf{u} = 2\pi A_e \mathbf{B}_e^T \mathbf{u}\, \boldsymbol{\sigma_{damaged}}, \tag{3.28}$$

where $\mathbf{P}$ stands for the $6x1$ vector of internal forces corresponding to the appropriate code numbers.

Whole procedure is summarized in the following schematic flowchart (Fig. 3.14).

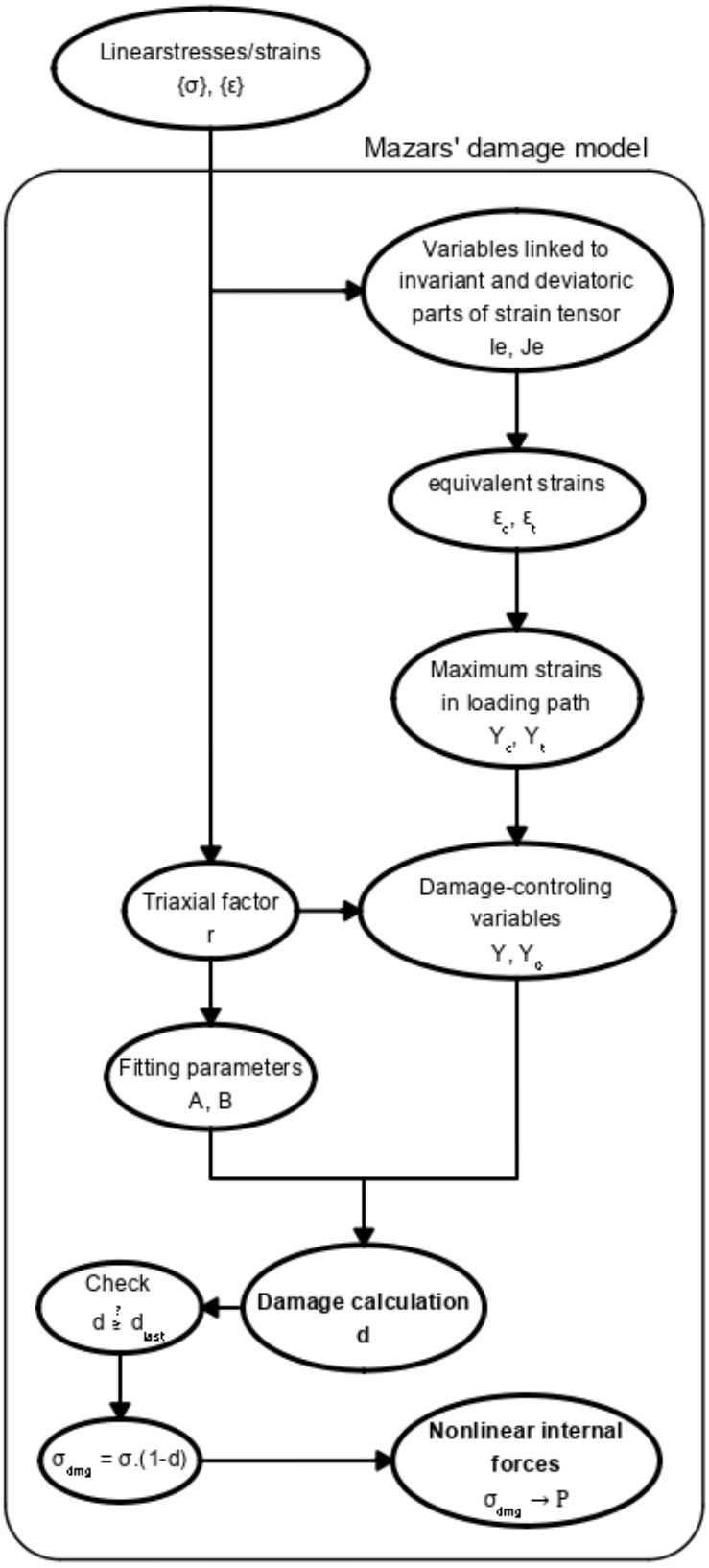

Figure 3.14: Flowchart of nonlinear analysis - determination of damage using Mazars' μ damage model

3.5.3 Fitting model parameters using a virtual compression test

As was mentioned in the previous section, the Mazars' μ model of damage need certain input parameters to describe the nonlinear behavior properly. Fitting of these parameters usually takes place after the real experiments are performed and the actual stress-strain diagram obtained.

The experiments are not part of this work. However, a virtual experiments (compression and tension) were conducted to provide the desired result. A concrete cylindrical specimen of prescribed dimensions was considered (see Fig. 3.15).

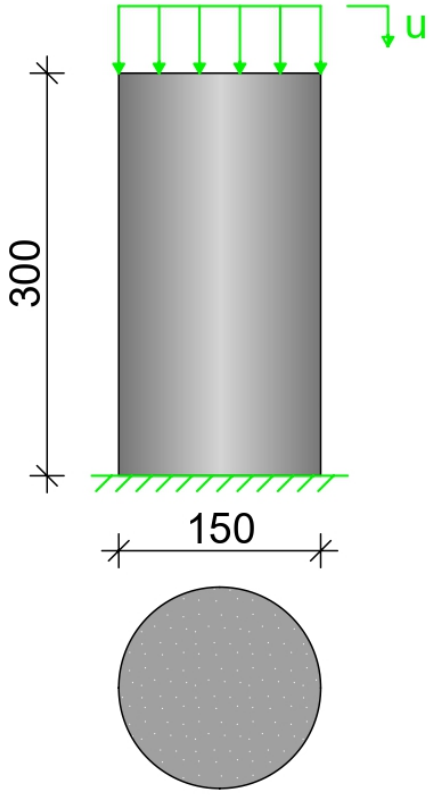

Figure 3.15: Cylindrical specimen used in virtual tests

Procedure of the response calculation was very similar to the CBS analysis, which provides another reason for the tests implementation - verification of the algorithm. The cylindrical specimen was considered axisymmetric with a close to zero radius for the reason to avoid possible mathematical errors e.g. dividing by zero in the **B** matrix.

Displacement-controlled loading

The main difference from the CBS analysis is the form of implementing the external forces. Whereas the CBS analysis is force-controlled procedure, the virtual tests are displacement-controlled. In general, the displacement control provides more stable and reliable option of analysis [19].

There are three popular methods for displacement control implementation: *Master-Slave Elimination, Penalty Augmentation and Lagrange Multiplier Adjunction* [22].

In the program, the last listed method was used. Principle of the *Lagrange Multiplier Adjunction* is basically adjoining an additional set of equations to the system of equations stating equilibrium of internal and external forces (Eq. 3.1). These equations represent the prescribed displacements assigned with appropriate code numbers. A new system is formed [22]:

$$\begin{pmatrix} \mathbf{K} & \mathbf{A^T} \\ \mathbf{A} & \mathbf{0} \end{pmatrix} \begin{pmatrix} \mathbf{u} \\ \boldsymbol{\lambda} \end{pmatrix} = \begin{pmatrix} \mathbf{f} \\ \mathbf{p} \end{pmatrix} \tag{3.29}$$

The $\mathbf{K}$ is the initial stiffness matrix, $\mathbf{u}$ is the vector of unknowns (displacements), $\mathbf{f}$ is vector of applied forces. The added "submatrix" $\mathbf{A}$ and its transposition $\mathbf{A^T}$ are so called *borders* of the stiffness matrix. The λ is called *Lagrange multiplier* and represents the desired forces of equal effect as the prescribed displacement. In displacement-controlled procedure, these forces in vector $\boldsymbol{\lambda}$ are the unknown (hence the position with the vector of unknown). And lastly, the $\mathbf{p}$ stands for the prescribed value of displacement. Dimensions of vectors $\boldsymbol{\lambda}$, $\mathbf{p}$ and matrix $\mathbf{A}$ unequivocally correspond to the number of nodes with a load applied in (or the number of code numbers representing the DoF). The principle implemented in algorithm is illustrated by the following picture (Fig. 3.16) and described process.

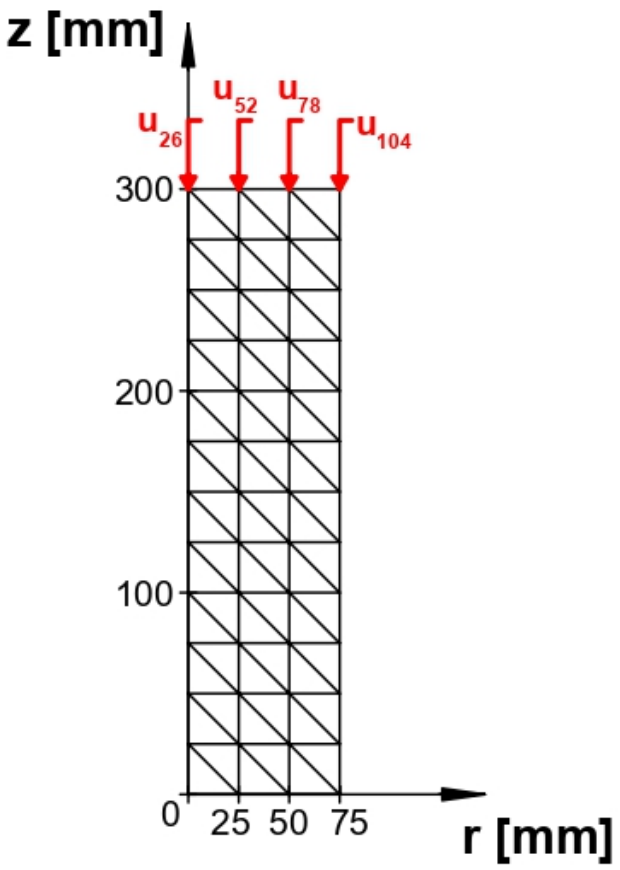

Figure 3.16: *Axisymmetric* FE model of the cylinder
under displacement-controlled load

It can be clearly seen in the picture that there is load applied in four nodes, therefore both vectors' $\boldsymbol{\lambda}$ and $\mathbf{p}$ dimensions are 4×1 and matrix $\mathbf{A}$ is $4 \times$ ($\mathbf{K}$ *dimension*). Components of $\boldsymbol{\lambda}$ are unknowns, in vector $\mathbf{p}$ are all equal to the prescribed displacement and $\mathbf{A}$ is full of zeros besides the columns corresponding to the code numbers (see Fig. 3.16) in each row. The adjunct system of resulted equations equations is:

$$u_{26} = u_{52} = u_{78} = u_{104} = u_{prescribed},$$

where $u_{prescribed}$ is a load applied in each step. The load was increased in each step from $0\,mm$ up to $0.94\,mm$ by $0.01\,mm$.

Parameter	Value	Units	Description
E	35	GPa	Young's modulus of elasticity
ν	0.2	-	Poisson's ratio
ρ	40	$\frac{kN}{m^3}$	Density
f_c	46.1	MPa	Ultimate compression strength
f_t	3.36	MPa	Tension strength
ε_{t0}	$1.25 \cdot 10^{-4}$	-	Initial threshold of ε_t (see Chapter 3.5)
ε_{c0}	$6.85 \cdot 10^{-4}$	-	Initial threshold of ε_c (see Chapter 3.5)
A_t	0.75	-	
A_c	1.75	-	
B_t	17 000	-	
B_c	105	-	

Table 3.1: Material and model parameters

Results of the tests

As a result, a stress-strain (force-displacement) diagram was obtained. Based on the shape and values reached during loading, the Mazars' μ model's parameters were fitted as well as the mesh refinement to be used in the CBS analysis. Used mesh is rather coarse (as can be seen in Fig. 3.16) due to using the same finite elements' size to reduce the effect of mesh dependency. Used parameters and overall material properties are summarized in the table above (Table 3.1).

The variables mentioned before were fitted so the desired compressive and tensile strengths were reached. Their value as well as the stress-strain (or force-displacement) diagram can be seen in the following figures (Fig. 3.17 or Fig. 3.18).

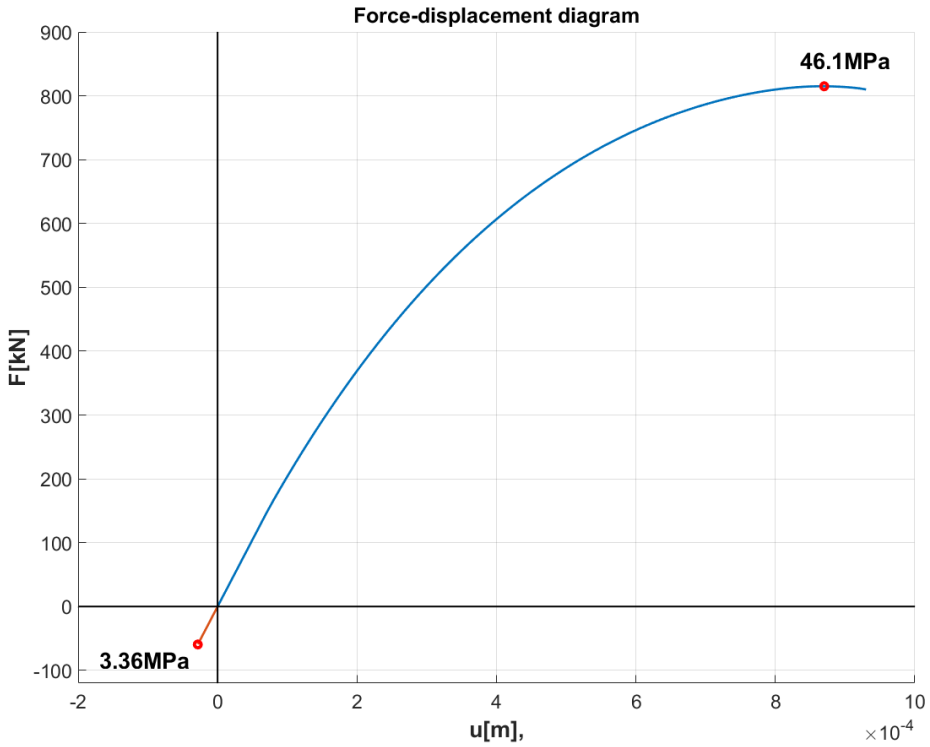

Figure 3.17: Force-displacement diagram using fitted parameters (with highlighted max. strength)

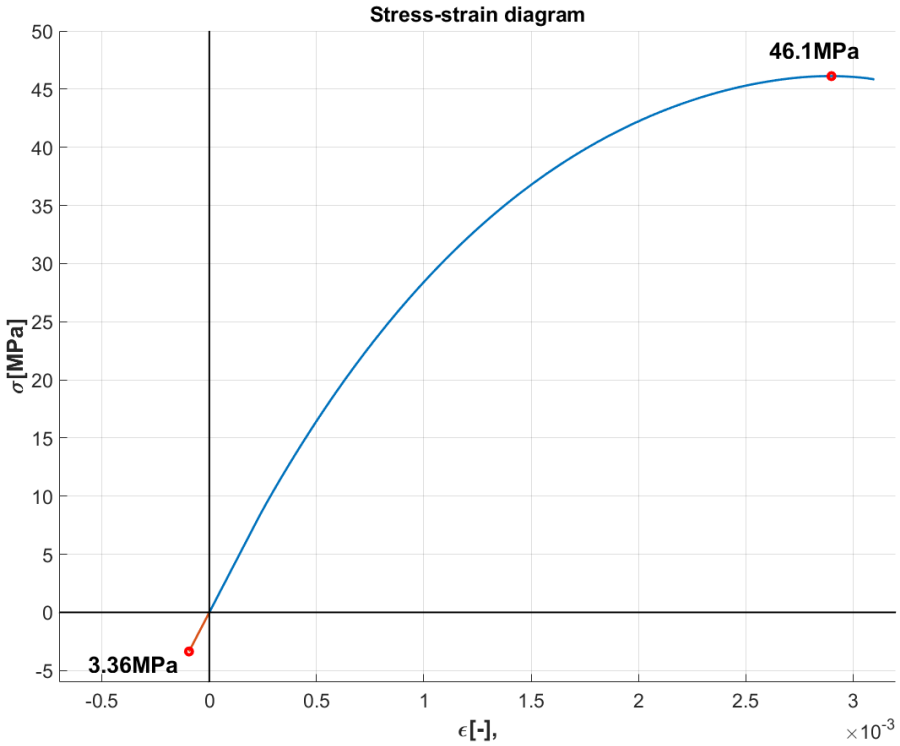

Figure 3.18: Stress-strain diagram using fitted parameters (with highlighted max. strength)

CHAPTER 4

Results and Comparison with other models

As was stated earlier, the key requirement of the CBS is its soundness, therefore cracks restriction. And for that reason, the main goal of the analysis was to determine time after which a damage appears and how it develops over the years of operation of the reactor.

The damage evolution is illustrated by the following pictures (Fig. 4.1 and Fig. 4.2). Fig. 4.1 shows that first signs of damage appear already after six years of reactor's operation, which is rather early in comparison with other models (this behavior is described with more detail in the following section - particularly Chapter 4.3) and also the fact, that the important value of neutron radiation dosage (neutron fluence of $1 \cdot 10^{19}\ n/cm^2$) is reached after 10 years (described with more detail in Chapter 2.2.1). Damage origins in the upper part of the section, although the maximal effect of RIVE is in the close-to-middle part, the firmness of the upper part is reduced by the change of the section geometry. Minimum thickness of this part is 100 mm, while the full thickness of the body is 700 mm. Followed up by Fig. 4.2, the evolution of the damage can be seen. The damage develops along the inner surface rather rapidly.

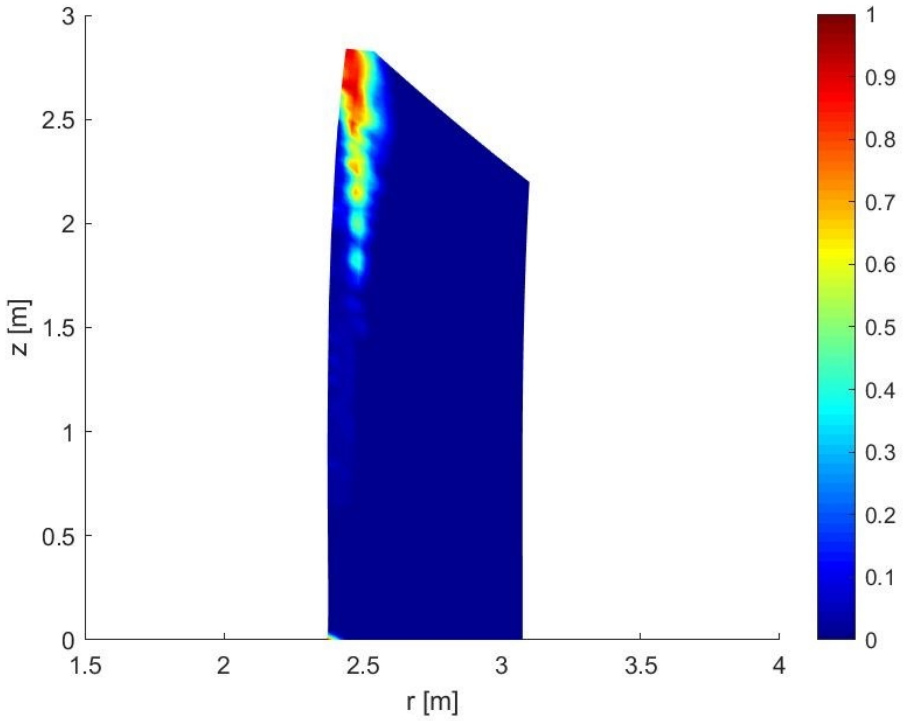

Figure 4.1: Damage reaches value of 1.0 after 6 years of operation

Both - time of damage origin and the speed of development - can be mostly explained by neglecting the effect of creep in analysis, which is relatively important in this case due to reducing stiffness of the structure, in other words, the structure is more flexible and therefore smaller stresses are generated (which also directly results from the equation Eq. 3.3). The creep of the concrete is a phenomenon of a long-term character, which comes hand in hand with irradiation effect that continues multiple years, more precisely decades. This impact of creep on irradiated structures is confirmed also by the publication by *Giorla, Le Pape and Dunant (2017)* [23] and the reduction of cracks' width is also mentioned in [24]. Last but not least, another reason for contradiction of the results is neglecting influence resulted from gamma and neutron irradiation (e.g. stiffness and strengths reduction) as well as from higher operational temperature and moisture. Also, some phenomena may be lost on the account of the assumption of axisymmetric model, which is a way of simplification.

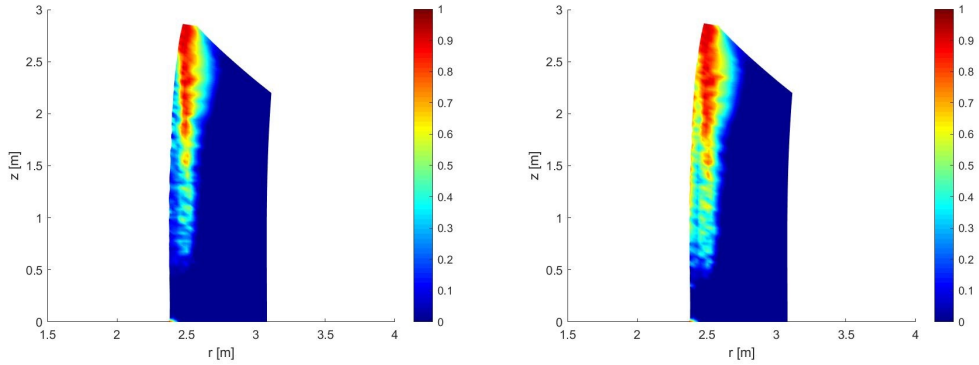

(a) Damage evolution after 10 years of operation

(b) Damage evolution after 13 years of operation

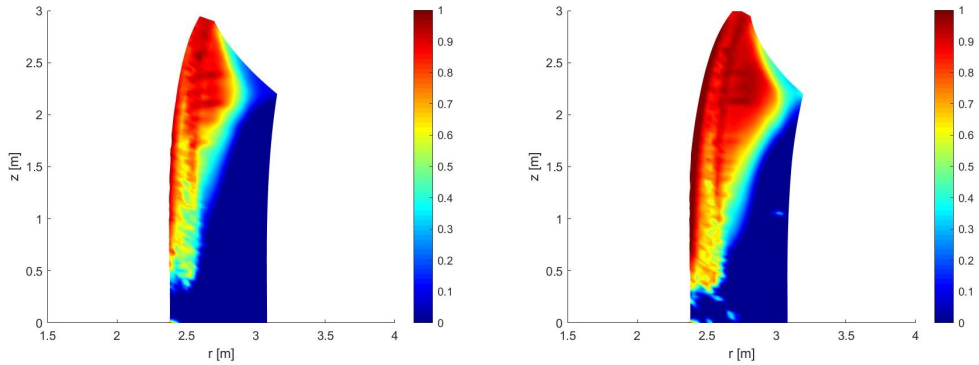

(c) Damage evolution after 30 years of operation

(d) Damage evolution after 60 years of operation

Figure 4.2: Damage evolution in the cross-section of the analysed CBS

Lastly, the mesh dependency may also play an important role. For example, it can be witnessed in comparison of the evolution of damage on the following figures (Fig. 4.3a and Fig. 4.3b) and in the result in Chapter 4.1, where damage progresses from the top as well, but not that rapidly at all - the smaller, less firm part of the section may be more susceptible to mesh dependency. To reduce the model's dependency on mesh refinement, the non-local approach [25] should be implemented when calculating damage. This approach will be done in the future work. The mesh dependency is demonstrated by following pictures (Fig. 4.3a and Fig. 4.3b) that compare two results with all aspects (load, load steps, material parameters, etc) of the same value with a single difference - structure in the picture on the right has finer mesh than the one on the left picture. Difference of the results

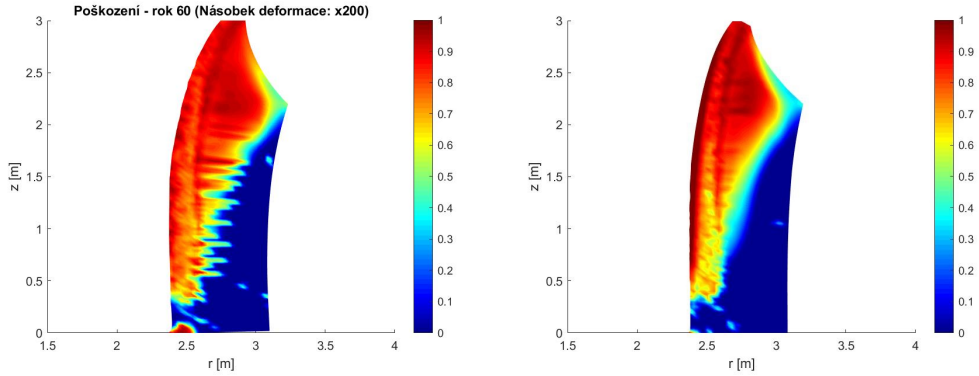

(a) Damage after 60 years - construction with **coarse** mesh

(b) Damage after 60 years - construction with **finer** mesh

Figure 4.3: Testing mesh dependency on 60-years damage

confirms that the model is mesh dependent.

There is one more noticeable aspect of the damage evolution in figures Fig. 4.2c and Fig. 4.2d. That is a form of "discontinuity" of damage in the r direction. The "first part" that originates from the inner surface of CBS seems to agree with results in publications introduced in Chapter 4.1 and Chapter 4.4.

On the topic of irradiated concrete, a number of models were created in last $\approx$ 10 years. Two levels of models are distinguished: microscopic level, studying usually effect on the individual components, and macroscopic level, models of the whole irradiated structure. A few publications are dedicated to analysing the structure as a whole, comparatively as this thesis. In the individual sections of this chapter, four of such models are briefly introduced, compared to the model created for this thesis (or its modification - Chapter 4.1) and the reasons for results differences are given.

4.1 3D RBSM analysis - *Kambayashi, Sasano, Sawada, Suzuki, Maruyama (2020)*

In publication by mentioned authors in 2020 [24], a 3D rigid body spring model (RBSM) of cylindrical concrete biological shield is proposed to simulate deterioration under exposure to gamma and neutron radiation based on previous experimental investigation.

A RBSM uses discontinuous elements, unlike FEM, therefore behavior, such as crack evolution, is fairly easily modeled. The model considers more components (aggregates, mortar) as individual elements rather than only a homogeneous material (like in the next introduced models), which allows application of the effect of irradiation more accurately. The reinforcement of the concrete and the inter-facial transition zone are also considered. The analysis also includes RIVE, thermal strain, creep and internal steel liner.

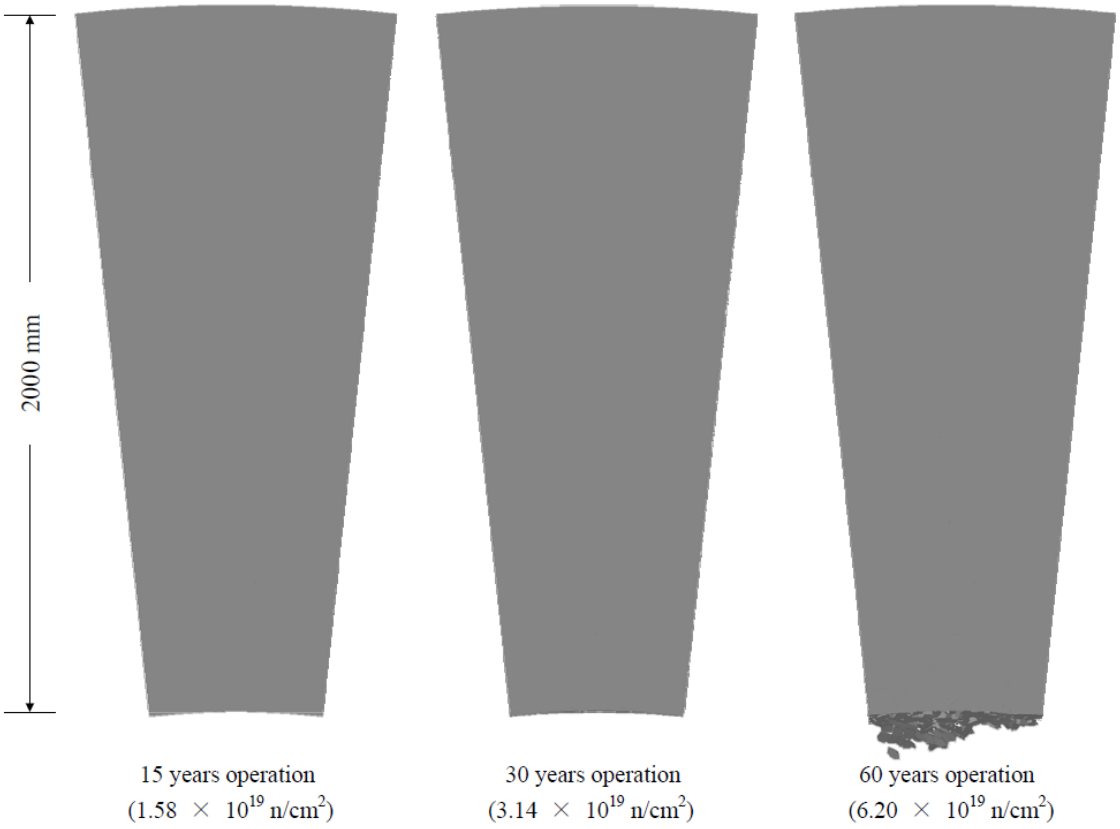

Figure 4.4: Deformation of the part of the CBS after 15/30/60 years of operation and occurrence of the cracks

The results of this analysis show that after 30 years of operation, the cracks start to form near the inner surface, which then expand in the circumferential direction. And after 60 years, the surface layer begins to "crumble" (see Fig. 4.4).

With all the factors included in the analysis listed earlier plus the fact that the geometry difference and load applied (presented CBS is not only self-bearing, but it supports the pressure vessel of the reactor - additional vertical load), it is not possible to compare results from the introduced RBSM model and the created axisymmetric model. And lastly, the conclusion of discussed publication is that the cracks evolve in the circumferential direction (noticeable in Fig. 4.5), which is impossible to take into account using axisymmetry by its principle.

However, the algorithm was used on a similar structure to at least get closer look at the comparison. The CBS is considered to be a cylindrical structure with thickness of 2 m. Damage within this structure appears to behave relatively more accurately than in Chapter 4, which might also indicate that the geometry

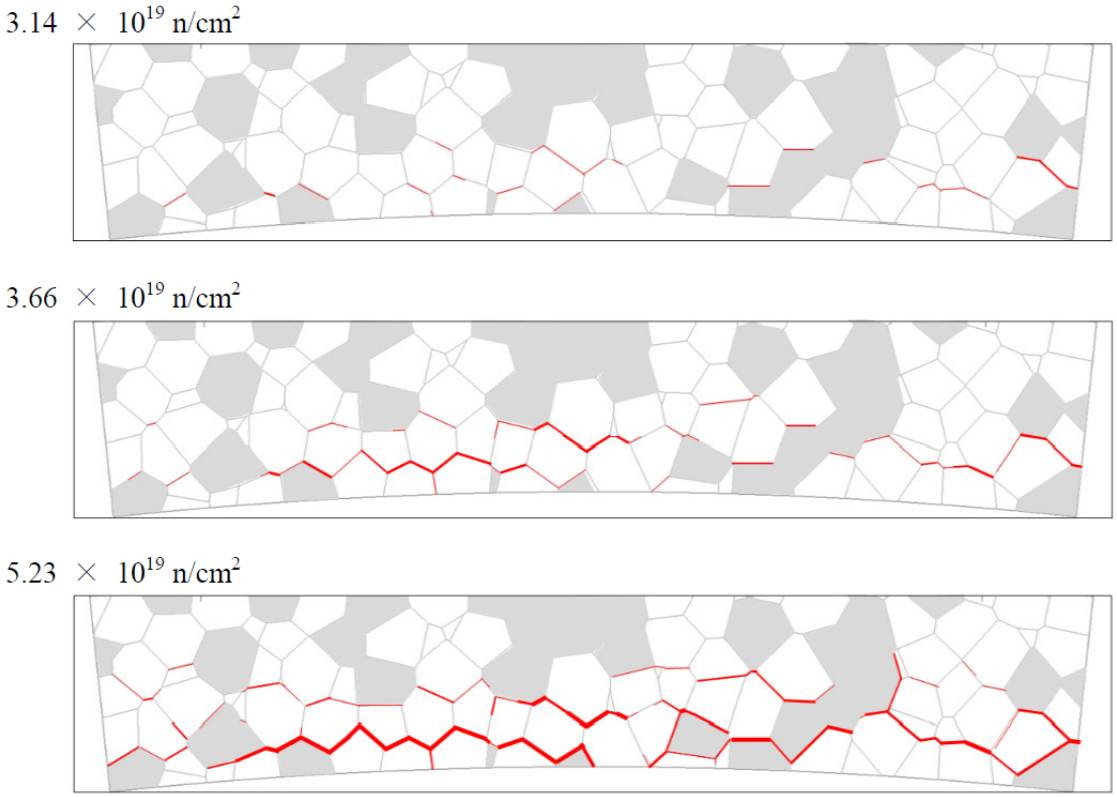

Figure 4.5: Cracks growth in the circumferential direction
from 30 up to ≈ 55 years of operation

of VVER 440/213 CBS wall is more sensitive to mesh dependency than this structure with times bigger stiffness, although these results (Fig. 4.6a and Fig. 4.6b) seem to be closer to reality (meaning closer to results from the other analyses). Also, with closer look at the damage after 30 years of operation, the extend of damage is much less severe than the one in the analysed CBS results in Chapter 4. However, the "discontinuity" between the "layers of damage" appear again. In certain elements, damage reaches the maximum values of 0.97, which suggests that the crack starts to form, comparatively as in the RBSM analysis. These can be another arguments for the necessity of implementing the non-local approach in the algorithm as was discussed earlier in this chapter.

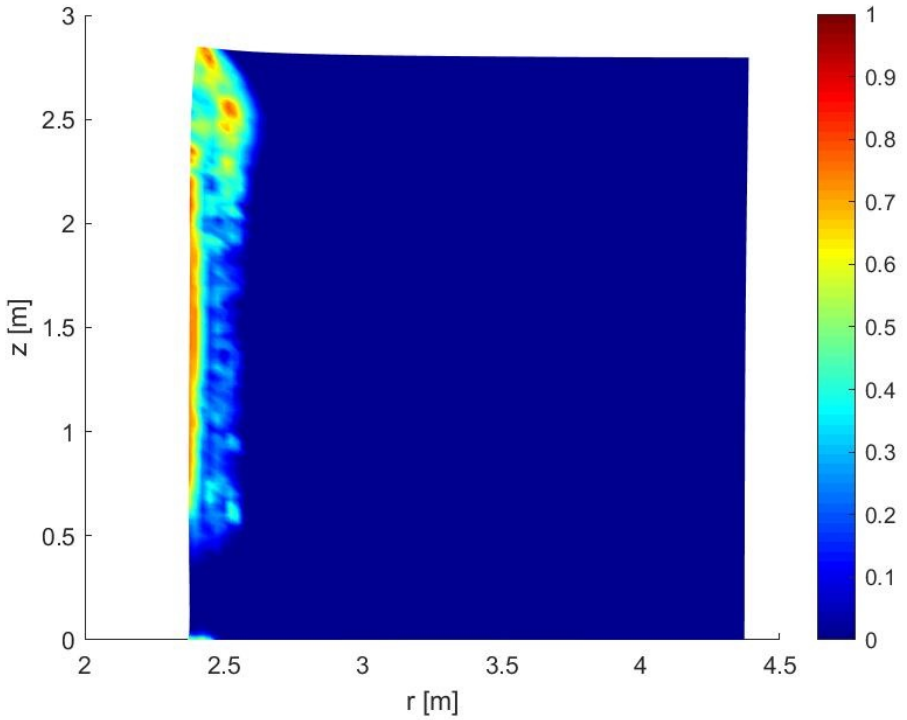

(a) Damage after 15 years of operation

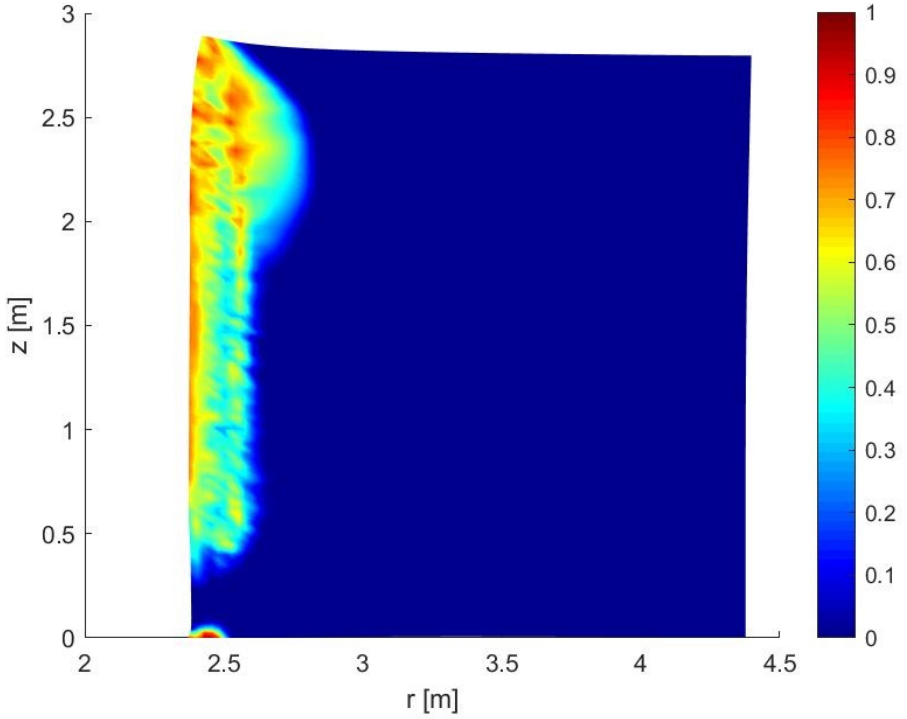

(b) Damage after 30 years of operation

Figure 4.6: Damage evolution after applying the created algorithm on the structure of similar shape

4.2 Evaluating methods for the CBS, an FE analysis - *Bruck, Esselman et al. (2019)*

Mentioned authors published an article rather on establishing assessment and evaluation methods of structures affected by aggressive environment associated with shielding radiation. [18]

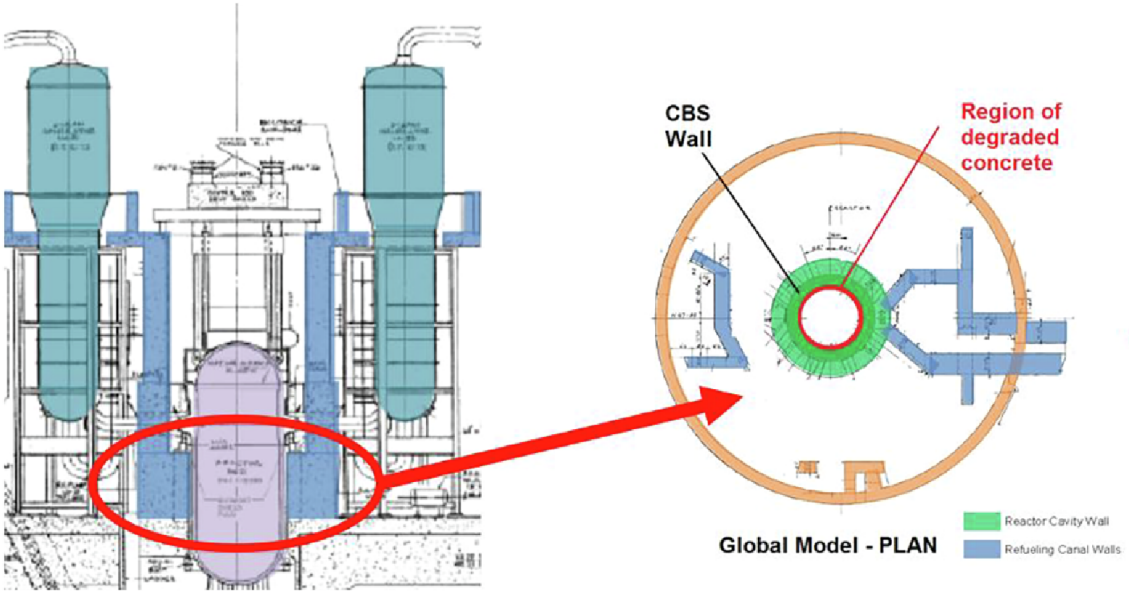

Figure 4.7: CBS considered by *Bruck et al. 2019* study, highlight of the most damaged part (surface on the inner diameter)

This publication studies a CBS in the form of a cylindrical structure with reinforcement supporting the reactor pressure vessel (schema in Fig. 4.7 [18]) by creating an FE model using ANSYS software. Similarly to models in Chapter 4.1 and Chapter 4.4 (given the fact that the boundary conditions, applied load and concrete properties changes taken into account are alike), results of this article match in the part that the inner part (inner surface) of CBS being the most deteriorated (highlighted in Fig. 4.7). This study, however, points out that cracks can appear on the outer surface of CBS caused by tensile stresses as a reaction to the compression stresses in the inner part as a result of RIVE, unlike Kambayashi, Maruyama et al. who contradict this statement in [24] and suggest that the stresses on the outer surface are of no importance. On the other hand,

Le Pape in [12] shows that the tensile stress in circumferential direction can reach values larger than 5 MPa (see Fig. 4.11 in Chapter 4.4).

The Fig. 4.8 presents the principle tensile stresses in the CBS model described in previous section, analysed by the program created in this thesis. It shows that the stresses near the outer surface are of no significance (more precisely, they do not exceed the tensile strength of concrete, therefore no cracks appear).

This differences in results can be caused by different vertical loads representing the reactor pressure vessel. Kambayashi, Maruyama et al. directly mentions the value of applied load being constantly 1 MPa on the upper surface of the cylinder. Bruck, Esselman et al. and Le Pape do not mention directly the certain vertical load. The created model of this thesis does not take into account load by the pressure vessel, however a fairly dense concrete ($\rho = 40\ kN/m^3$) is considered, which generates certain non-negligible vertical load as well. So it is possible that this conclusion depends on the vertical force stabilizing the structure.

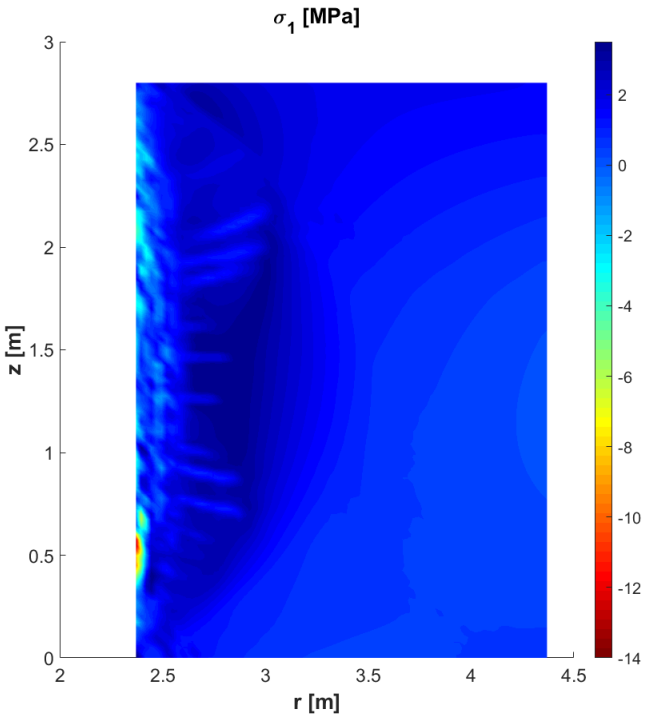

Figure 4.8: Principle tensile stresses in the model of CBS with modified geometry

4.3 3D FE analysis of the CBS of VVER 440/213 - *Khmurovska (2019)*

The 3D model proposed by Khmurovska for an FE analysis and mainly assessment of damage development used in [11] provides probably the most useful example in order to compare analysis conducted during this thesis due to considering structure of the same geometry. Results of the analysis show that the first cracks appear in the upper part of the section in the circumferential direction after 12.75 years of operation (Fig. 4.9 [11]).

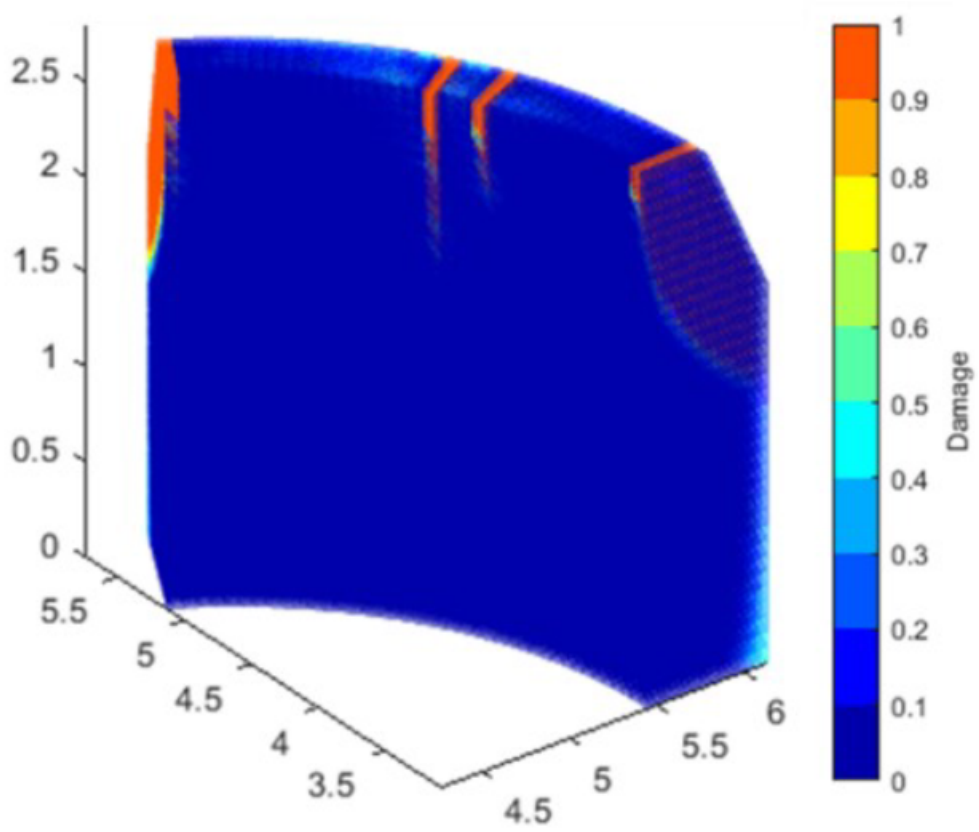

Figure 4.9: Damage appearing after 12.75 years of operation

The part where it first occurs corresponds to what the results in the beginning of this chapter suggest as well. However, the direction seem to represent a problem for using axisymmetric assumption, which would predict damage in every single section of the structure. The assumption also considers adjusted coarse of neutron fluence

in the horizontal direction (as was explained in Chapter 3.4). This indicates the importance of a three-dimensional FEA, which is also one of the recommendations given by Le Pape in [7].

The part of the section where damage propagation originates corresponds with the results presented earlier, although the time of origin varies. In the results shown, the damage occurs much earlier - after 6 years (Fig. 4.1) - and after 13 years (load was applied in steps correlating with whole years, hence the 13 years figure, Fig. 4.2b) is fairly progressed. This is most probably due to neglecting many aspects that are considered in Khmurovska's analysis (concrete creep, other effects of gamma and neutron irradiation, impact of temperature, etc) as well as implementing the local approach of damage determination.

4.4 1D model - *Le Pape 2015*

Another example of similar analysis is Le Pape's one-dimensional model of a CBS. The considered dimension is in the direction of radius (r), therefore the main unknown (displacement u) is driven only by one variable ($u = f(r)$) [7]. The model considers a belt line region of a 1.5 m-thick wall without reinforcement (see Fig. 4.10 [7]), considers 80 years of operation and takes into account another effects of irradiation such as decrease of Young's modulus, strengths reduction or the effect of the operational temperature.

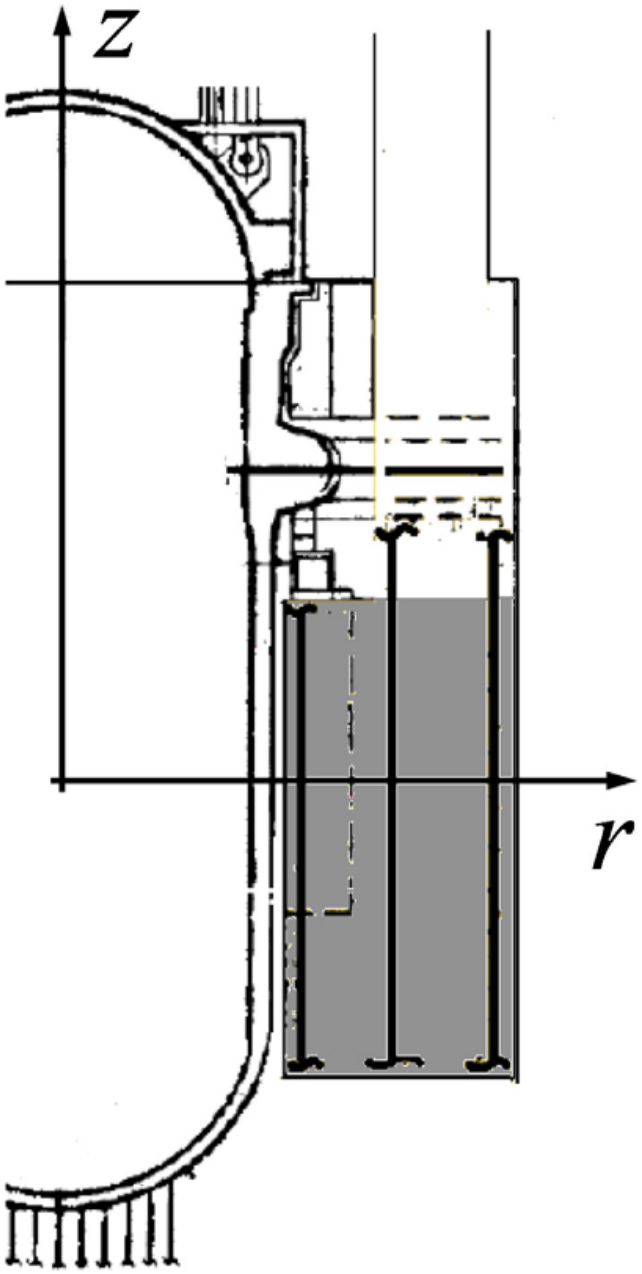

Figure 4.10: Schema of the model of the CBS considered by Le Pape

After this time of operation, the stresses in separate directions are evaluated (see Fig. 4.11 [7]). The stress in vertical and circumferential direction are fairly significant into depth of ≈ 300 to 400 mm, which agrees with the analysis mentioned in Chapter 4.1, where the stresses are significant as far as ≈ 250 to 300 mm inside the CBS. The slight difference can be explained by [24] taking rebar into account, while [7] considers unreinforced concrete.

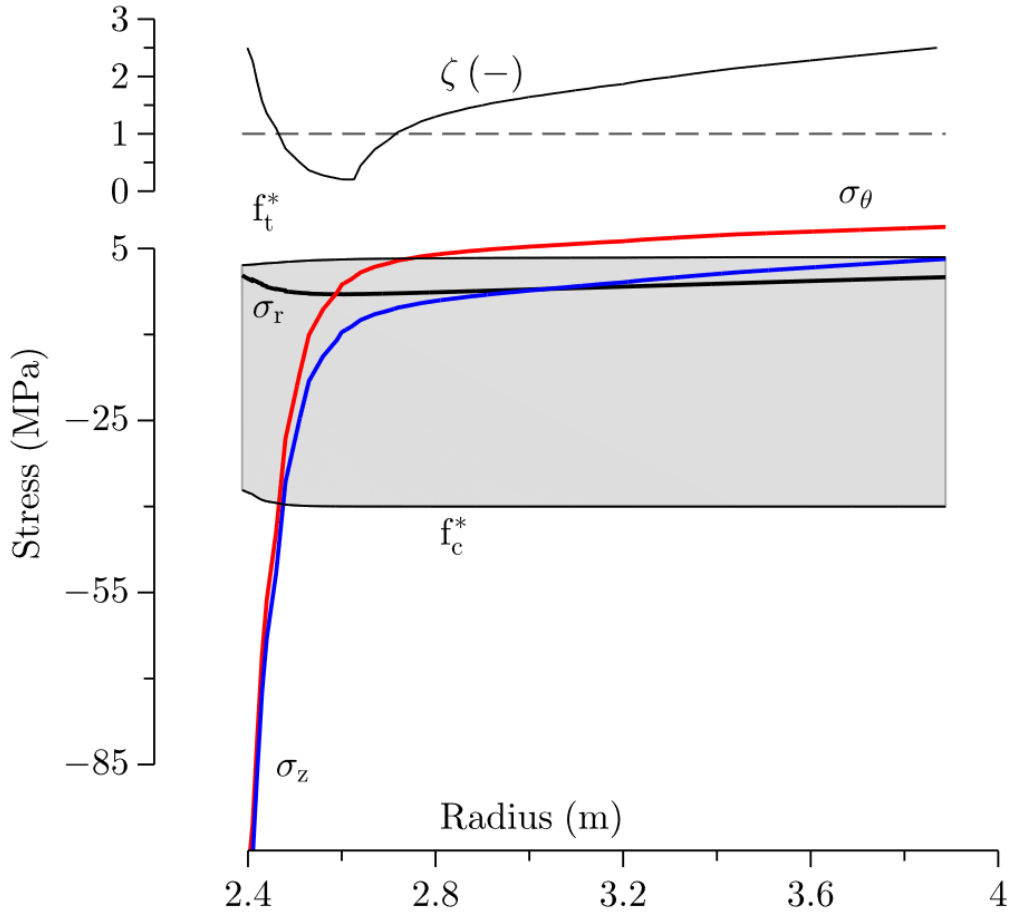

Figure 4.11: Distribution of stresses over the thickness inside the CBS

After applying created algorithm on the modified geometry (Chapter 4.1) that is closer to the one used in this analysis, the depth of stresses after 60 years of operation is ≈ 70 mm (Fig. 4.12 shows the depth of non-negligible σ_{cir}). The difference can be caused by more aspects: Le Pape's model considers 80 years of operation, the created program considers 60 years and Le Pape's model also takes into account all the effects listed above, which are excluded from analysis in this thesis.

The author also highlights that the results confirm the importance of RIVE and it being the main cause of damage propagation: "*Interestingly, when RIVE is not accounted for, no damage propagation is found...*" [7]

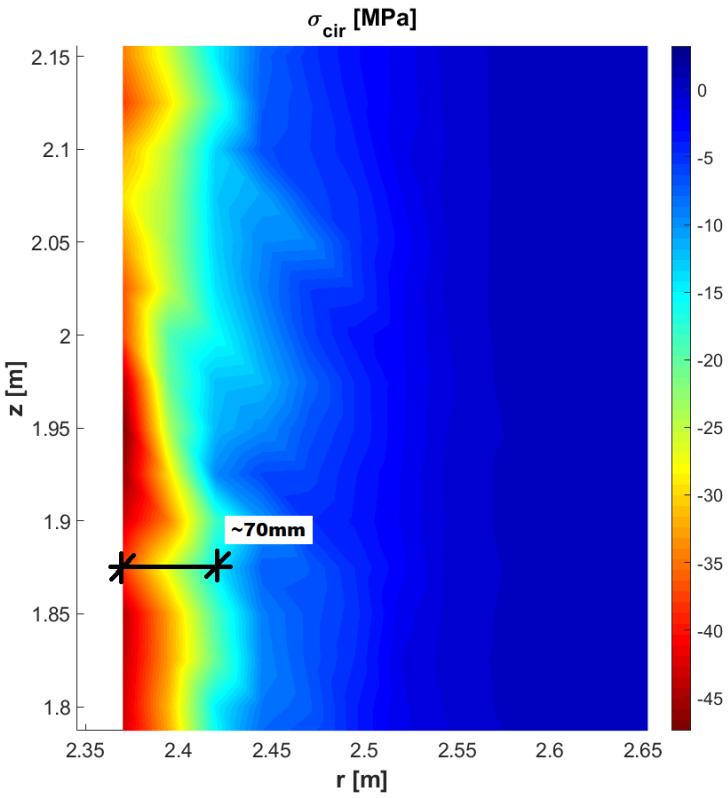

Figure 4.12: Depth of circumferential stress on CBS with modified geometry

CHAPTER 5

Conclusion

Goal of this thesis was a numerical analysis of a concrete biological shield (CBS) of a reactor type VVER 440/213 exposed to RIVE, phenomenon caused by neutron irradiation. Axisymmetric model of the structure was assumed, the nonlinear analysis using finite element method was conducted, focusing on determination of evolution of damage of the structure. Modified Newton-Raphson iteration method was used for nonlinear calculation with Mazars' μ damage model describing nonlinear behavior of concrete.

Results presented in Chapter 4 show that first signs of damage occur already after six years of operation, which is relatively early considering the designed operating lifespan of a reactor. This fact is confirmed also by other models introduced in Chapter 4, suggesting that the damage originates in the same part, but a few years later. This can be caused by neglecting some of the effects, especially creep that can have a non-negligible impact on the calculated stresses in order of an analysis simulating several-years operation. Some of the introduced works (Bruck, Esselman et al. [18] and Maruyama et al. [24]) conduct similar analysis of a structure with a different geometry. The created algorithm was used on a structure

after geometry modification in order to resemble the structure in listed publications.

Major reason for the results difference can be essentially the following two aspects: neglecting other effects, which are considered by other models and mainly then unresolved *mesh dependency* that could be a source of uncertainties with the original geometry as well as the unusual shape of damage showed in Chapter 4. The created algorithm considers a local approach of damage determination, although implementation of the non-local approach would reduce the mesh dependency of the model. This is planned to be added to the model, as well as additional effects of radiation, in the course of future work.

Bibliography

[1] Mycle Schneider, Antony Froggatt, Julie Hazemann, Tadahiro Katsuta, and MV Ramana. The world nuclear industry status report 2022. *Paris: Mycle Schneider Consulting*, 2022.

[2] Yann Le Pape, Julien Sanahuja, and Mustafa HF Alsaid. Irradiation-induced damage in concrete-forming aggregates: revisiting literature data through micromechanics. *Materials and Structures*, 53(3):1–35, 2020.

[3] H.K. Hilsdorf, J. Kropp, and H.J. Koch. The effects of nuclear radiation on the mechanical properties of concrete. *Special Publication*, 55:223–254, 1978.

[4] Aleksander Samarin. Use of concrete as a biological shield from ionising radiation. *Sustainable Construction Materials and Technologies*, 2013.

[5] Leonard Hobst, Jan Jašek, and Lubomír Vítek. Těžké betony a speciální stínící betony — heavy concrete and special shielding concrete. *Časopis Beton*, pages 135–140, 2012.

[6] A. Denisov, V. Dubrovskii, and V. Solovyov. Radiation resistance of mineral and polymer construction materials. *ZAO MEI Publ. House*, 2012.

[7] Y. Le Pape. Structural effects of radiation-induced volumetric expansion on unreinforced concrete biological shields. *Nuclear Engineering and Design*, 295:534–548, 2015.

[8] P. Bouniol and A. Aspart. Disappearance of oxygen in concrete under irradiation: the role of peroxides in radiolysis. *Cement and concrete research*, 28(11):1669–1681, 1998.

[9] Ippei Maruyama, Shunsuke Ishikawa, Junichi Yasukouchi, Shohei Sawada, Ryo Kurihara, Masayuki Takizawa, and Osamu Kontani. Impact of gamma-ray irradiation on hardened white portland cement pastes exposed to atmosphere. *Cement and Concrete Research*, 108:59–71, 2018.

[10] Y. Kitsutaka and K. Matsuzawa. The effect of gamma radiation on the fracture properties of concrete. *Fracture mechanics of concrete and concrete structures—Recent Advances in Fracture Mechanics of Concrete, FramCoS-7*, pages 23–28, 2010.

[11] Yuliia Khmurovska, Petr Štemberk, Tamáš Fekete, and Tapani Eurajoki. Numerical analysis of VVER-440/213 concrete biological shield under normal operation. *Nuclear Engineering and Design*, 350:58–66, 2019.

[12] Daryl L Logan. *A first course in the finite element method*. Cengage Learning, 2016.

[13] G. K. Ananthasuresh. Online notes for fea, available online at: `https://mecheng.iisc.ac.in/suresh/me237/notes.html`. Accessed: 2023-01-03.

[14] Radim Blaheta. Matematické modelování a metoda konečných prvků. *Matematika pro inženýry*, 21, 2012.

[15] Shriram Hegde. Online notes for course apl705 finite element method, available online at: `https://web.iitd.ac.in/~hegde/fem/index.html`. Accessed: 2023-01-03.

[16] Pavel Zácha. Vyšetřování trojrozměrného proudového a teplotního pole v sestupné šachtě a dolní směšovací komoře reaktoru VVER-440. 2008.

[17] Y. Khmurovska and P. Štemberk. FEM and RBSM numerical analysis of concrete wall under long-term exposure to neutron irradiation. In *Proceedings of the 12th International PhD Symposium in Civil Engineering, Prague, Czech Republic*, 2018.

[18] P.M. Bruck, T.C. Esselman, B.M. Elaidi, J.J. Wall, and E.L. Wong. Structural assessment of radiation damage in light water power reactor concrete biological shield walls. *Nuclear Engineering and Design*, 350:9–20, 2019.

[19] Nam-Ho Kim. *Introduction to nonlinear finite element analysis*. Springer Science & Business Media, 2014.

[20] Jacky Mazars. A description of micro-and macroscale damage of concrete structures. *Engineering Fracture Mechanics*, 25(5-6):729–737, 1986.

[21] Jacky Mazars, François Hamon, and Stéphane Grange. A new 3d damage model for concrete under monotonic, cyclic and dynamic loadings. *Materials and structures*, 48(11):3779–3793, 2015.

[22] Carlos A. Felippa. Introduction to finite element methods. *University of Colorado*, 885, 2004.

[23] Alain B. Giorla, Yann Le Pape, and Cyrille F. Dunant. Computing creep-damage interactions in irradiated concrete. *Journal of Nanomechanics and Micromechanics*, 7(2):04017001, 2017.

[24] Daisuke Kambayashi, Hiroshi Sasano, Shohei Sawada, Kiyoteru Suzuki, and Ippei Maruyama. Numerical analysis of a concrete biological shielding wall under neutron irradiation by 3d rbsm. *Journal of Advanced Concrete Technology*, 18(10):618–632, 2020.

[25] Gilles Pijaudier-Cabot and Jacky Mazars. Damage models for concrete, 2001.